NONLINEAR DESIGN, MODELING AND SIMULATION OF MAGNETO RHEOLOGICAL SUSPENSION: A CONTROL SYSTEM AND SYSTEMS ENGINEERING APPROACH

A Thesis

Submitted to the Faculty

of

Purdue University

by

Hrishikesh B. Zambare

In Partial Fulfillment of the

Requirements for the Degree

of

Master of Science in Mechanical Engineering

December 2017

Purdue University

Indianapolis, Indiana

THE PURDUE UNIVERSITY GRADUATE SCHOOL
STATEMENT OF COMMITTEE APPROVAL

Dr. Ali Razban, Co-Chair

Department of Mechanical Engineering

Dr. Hazim El-Mounayri, Co-Chair

Department of Mechanical Engineering

Dr. Jie Chen

Department of Mechanical Engineering

Approved by:

Dr. Sohel Anwar

Chair of Graduate Program

To my Mom, Dad, Sister, and Visha

ACKNOWLEDGMENTS

I would like to express my sincere gratitude towards my research advisor Dr. Ali Razban for his unyielding guidance, immense knowledge, and support towards the completion of my thesis. I want to thank him for having faith and belief in me and helping me out at each step. My sincere thanks goes to Surendra Patil and Abhishek Khoje for their precious support and help throughout my research work and leisure time, and making this journey memorable. I am gratefully indebted towards my parents, Mr. Balasaheb Zambare and Mrs. Sangita Zambare for inspiring me to aim higher and try harder throughout my graduate studies and my thesis research. This accomplishment would not have been possible without their encouragement. Thank you. I would also like to acknowledge my betrothed, Vishakha Modak, who has emboldened the passion and determination in me at each stage. Without her continuous moral support and love, this wouldnt have been such an amazing journey.

TABLE OF CONTENTS

Page

Page

LIST OF TABLES

LIST OF FIGURES

Figure Page

ABBREVIATIONS

BDD	Block Definition Diagram
FAST	Functional Analysis System Techniques
IBD	Internal Block Diagram
MBSE	Model Based Systems Engineering
MR	Magneto-Rheological
par	parametric
req	requirements

NOMENCLATURE

A	Road since wave amplitude
Ap	Damper cylinder core area
Cs	Damper Co-efficient
Cu	Tire Damping Co-efficient
C0a	C0b Bouc-Wen Model constants
F0	Pre-yield stress of damper
F_c	Frictional force loss in MR damper
Fmr	Force provided by MR damper
Fmax	Maximum damping force
fr	Road vibration frequency
Fs	Spring Frequency
F, Fv	Current dependent and viscous damping forces
g	Gap Thickness
I	Current through coil
K, Kwa	Hysteresis Loop Shape parameters
Kwb,	Hysteresis Loop Shape parameters
Ks	Suspension Spring stiffness
Ku	Tire Stiffness
L	Pole length
MR	Motion Ratio
Ms	Sprung Mass
Mt	Total Magnetic Reluctance
Mu	Unsprung Mass
Nc	Number of coil turns

Q	Damping fluid flow rate
R	Piston Radius
r	Road bump magnitude
r	Road bump profile derivative
r	Road bump profile integration
t	Cylinder Thickness
Uc	Controller Force
v	Control Voltage
w	Dynamic Hysteresis Co-efficient
W	Dynamic hysteresis Co-efficient derivative
x_P	Piston length
y	Evolutionary variable
Zs	Sprung Mass displacement
(Z_s)	Sprung Mass velocity
(Z_s)	Sprung Mass acceleration
Zu	Unsprung Mass displacement
(Z_u)	Unsprung Mass velocity
(Z_u)	Unsprung Mass acceleration
α, β, γ	Bouc Wen model constants
ϕ	Magnetic Flux
μ	Base viscosity of fluid
τy	Yield shear stress of MR fluid
ζmin, ζmax	Minimum and maximum damping ratios

ABSTRACT

Zambare, Hrishikesh B. M.S.M.E., Purdue University, December 2017. Nonlinear Design, Modeling and Simulation of Magneto Rheological Suspension: A Control System and Systems Engineering Approach. Major Professor: Ali Razban

Suspension has been the most important subsystem of the vehicle viewed as a system. The ride comfort and vehicle handling performance are affected by the suspension design. Automotive technology has been continuously incorporating developments over the past few decades to provide the end users with a better comfort of driving. Multi-objective optimization of MR damper with objective function of maximizing damping force generated by MR damper with the geometrical parametric constraint function is achieved in this research using pattern search optimization technique.

Research focuses on design, modeling, and simulation of active suspension using non-linear theory of the Magneto-Rheological (MR) damper with consideration of the hysteresis behavior for a quarter car model. The research is based on the assumption that each wheel experiences same disturbance excitation. Hysteresis is analyzed using Bingham, Dahls, and Bouc-Wen models. Research includes simulation of passive, Bingham, Dahl, and Bouc-wen models. Modeled systems are analyzed for the six road profiles, including road type C according to international standards ISO/TC108/SC2N67. Furthermore, the comparative study of the models for the highest comfort with less overshoot and settling time of vehicle sprung mass are executed. The Bouc-Wen model is 36.91 percent more comfortable than passive suspension in terms of damping force requirements and has a 26.16 percent less overshoot, and 88.31 percent less settling time. The simulation of the Bouc-Wen model yields a damping force requirement of 2003 N which is 97.63 percent in agreement with analytically

calculated damping force generated by MR damper. PID controller implementation has improved the overshoot response of Bouc-Wen model in the range of 17.89 percent-81.96 percent for the different road profiles considered in this research without compromising on the settling time of system. PID controller implementation further improves the passenger comfort and vehicle ride handling capabilities.

The interdisciplinary approach of systems engineering principles for the suspension design provides unique edge to this research. Classical systems engineering tools and MBSE approach are applied in the design of the MR damper. Requirement traceability successfully validates the optimized MR damper.

1. INTRODUCTION

1.1 Research Objectives

Automotive technology has been continuously incorporating developments over the past few decades to provide the end users with a better comfort of riding. One such subsystem undergoing rigorous changes is the automotive suspension system, and the invention of electromagnetic capabilities of certain materials suspended in viscous oils has led to the development of the Magnetorheological (MR) damper technology. MR suspension has been an overwhelming technology in the past, where it could substitute the conventional damper system by a smart controlled damper to reduce sprung mass acceleration based on road profile conditions. MR fluid is responsible for the operational behavior and the significant performance changes in the MR damper. Magnetorheological fluids have recently been gaining popularity in automotive component applications such as engine mounts, clutches, brakes and nonetheless dampers for suspension systems [1, 2]. Controlling the motion of the vehicle body undergoing road profile variations has been a challenge to the engineering world owing to the complexities arising in multiple degree of freedom vibration response of the vehicle. Although electrically controlled suspension systems have been used to improve the dynamic performance of vehicles, such systems are still limited due to discontinuous damping forces, structural complexity, and high cost [3, 4]. MR dampers eliminate the requirement of a bulky reservoirs in the counterpart of pneumatic shock absorbers and come with an additional advantage of simple construction. MR dampers are essentially dampers with variable effective viscosity due to yield shear stress changes induced by excitation current controlled magnetic field strength in the damper coil [5, 6]. MR damper is a non-linear device with hysteretic characteristics, thus output of the MR damper is dependent on the previous outputs

and it is not solely on the instantaneous values [6]. Thus, the hysteretic study of the MR damper is carried out in this research considering four approaches; passive model without hysteresis, Bingham model, Dahls model, and Bouc-Wen model. The mathematical formulation for all the models are well established [7–9]. The comparative analysis illustrates the accurate model for design by comparing the force generated by the damper for the road disturbance characteristics at any given point of time. The analytical calculations part is the most critical phase of the design process as we define the MR damper parameters in terms of mathematical equations. This process involved the determination of spring force from values of quarter car mass, motion ratio of the vehicle, desired spring frequency and the damping ratio range [10]. The critical parameters of MR damper are determined using multi-objective optimization considering the critical parameters; pole length, piston radius, gap thickness, piston internal radius, piston velocity and coil current. The objective function constitute of damping force optimization for the desired damping force range, constrained with constraint on the critical design parameters. The controller implementation on MR active suspension for performance improvement is one of the important milestones on this research. Literature review witness that the PID controller holds the dominant position in industrial process control. The statistical data shows that PID controller implementation accounts for 84.5 percent and optimized PID controller accounts for 6.8 percent of the controllers used in the industry [11]. Also, the flexibility in structure set, parameter tuning, touch-type error, robustness, etc. allows a better control over the settling time, overshoot, damping factor, and steady-state error. Thus, PID controller is designed for the Bouc-Wen model, and the performance improvement is observed from the comparison of uncontrolled and controlled responses. Though the adequate amount of work has been done in the area controller implementation on the passive and active suspensions, controller implementation on the non-linear magnetorheological suspension system involving hysteresis loop would be the area of improvement. In the past, various suspension geometries have studied by researchers. The mathematical for wishbone suspension with conventional spring-mass-damper

system have been analyzed for the step change of spring stiffness and damping coefficient [12]. Also, PID controller was developed for each combination to analyze the suspension performance with respect to step road disturbance [12]. Advancement in this field led to replacement of conventional damper with controlled hydraulic dampers to provide a better road disturbance rejection and improvement in passenger comfort [13]. PID controller have been implemented on the active suspension system with hydraulic dampers [13]. The considered system for the study was with reduced degrees of freedom by elimination of tire damping [13]. A more robust and effective controller was developed for the hydraulic suspension considering the practical swarm optimization approach (PSO) [14]. High fidelity models for the quarter car suspension have been developed with intelligent system identification using the nonlinear autoregressive with eXogenous (NARX) input model. This system was tested for theoretical step road disturbance [15]. Further, advanced controls such as neural network based fuzzy logic was developed for the suspension performance improvement [16]. Also, back propagation neural (BPN) network approach for PID controller was developed for the active suspension control [17]. The recent advancement into the suspension technology incorporates the magneto-rheological (MR) damper for active suspension. Mathematical modeling and simulation automotive suspension with MR damper is developed with the elimination of hysteresis [18]. The hysteresis involved in the MR fluid is integral part of MR damper, which makes the system non-linear thus the consideration of hysteresis is important in the MR suspension design. Accurate representation and simulation of the suspension system must consider the tire damping in addition to damping provided through damper, hysteresis involved in the MR suspension, non-linear modeling of the system. Also, road disturbances considered play an important role in simulating actual operating conditions. This research illustrates the PID controller implementation on the magnetorheological suspension with Bouc-Wen theory of hysteresis. The system identification for hysteretic nonlinear suspension model is realized which is closer to the actual operating conditions. Furthermore, the developed and controlled system are tested for the six road profiles including

road type C according to international standards ISO/TC108/SC2N67 [11]. The system modeling, identification, controller implementation, and performance improvement are discussed in the subsequent sections. Viewing the MR active suspension with product development perspective, model based systems engineering approach (MBSE) approach is taken for the system development. OMG SysML is a general purpose language with an aid of graphical system representation used for specifying, analyzing, designing and verifying the complex system [19]. This graphical ability of SysML enables definition of many systems engineering concepts such as requirements, structure, functions, and behavior [20]. MBSE is approach has benefited the heath care, energy, and automotive industry to a great extent. Developed MBSE model also helps to validate the designed suspension system. MagicDraw system modeler is used for defining the MBSE model of active suspension MR damper. The major steps involved in the research are as follows: Mathematical modeling of quarter car active suspension using Bingham, Dahl, Bouc-Wen theory of hysteresis. Comparative study and simulation of suspension models with MR damper for the optimum model determination Analytical calculations of MR damper geometrical parameters considering the Bouc-Wen theory of hysteresis Sensitivity analysis of MR damper geometrical parameters Multi objective optimization of MR damper considering Bou-Wen theory of hysteresis PID controller implementation on active suspension comprising MR damper with Bouc-Wen theory of hysteresis MBSE approach for Bou-Wen suspension MR damper design FAST diagram approach for MR damper to define design features to meet functional requirements FMEA for determining the weak (uncontrollable) parameters in system design Value flow map preparation for identifying stakeholders and their needs Boundary diagram design for MR damper interface and interaction definition MBSE model development using requirements diagram, block definition diagram, internal block diagram, parametric diagram

1.2 Suspension System Overview

Suspension systems have been researched over a century by many researchers. Suspension system differs in the design and operation based on the control function and control principles. Primary segregation of the suspension has been done into passive suspension, semi-active suspension, and active suspension. These suspensions mainly differ into the damping force control mechanism for the experienced road disturbance.

1.2.1 Passive Suspension System

A vehicle's suspension system typically consists of springs and shock absorbers that help to isolate the vehicle chassis and occupants from sudden vertical displacements of the wheel assemblies during driving. A well-tuned suspension system is important for the comfort and safety of the vehicle occupants as well as the long-term durability of the vehicle's electronic and mechanical components [21]. The passive suspension system is a system in which the characteristics of the spring and the damper are fixed. The spring and damper characteristics are determined according to the performance goals and its intended application. The passive suspension system does not have capability of controlling suspension stiffness and damping coefficient according the road roughness or the disturbance amplitude. The figure 1.1 shows the typical schematics of passive suspension .

1.2.2 Semi-active Suspension System

Semi-active suspension has advantages over the passive suspension in terms of spring stiffness and damping coefficient control. Varying the spring stiffness for the particular design of the suspension is relatively difficult, and thus the semi-active working principle mainly focuses on the control of damping coefficient according to road roughness and disturbances experienced by the unsprung mass of the vehicle [21].

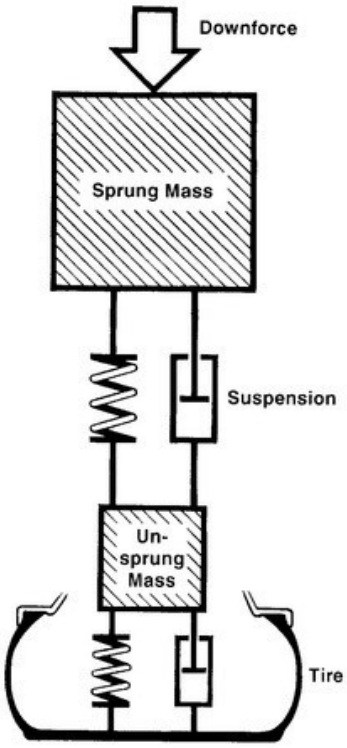

Fig. 1.1. Typical passive suspension schematics [22]

Semi-active suspension does not possess the separate dynamic control component for the operation of suspension against the road disturbances. Semi-active suspension process the road roughness/disturbances based on the suspension travel sensor feedback. The particular suspension states is baselined on the signals received from the road disturbances. Semi-active suspension system facilitates the better comfort to driver and passenger as compared to the passive suspension system. Also, controllable damper facilitates the improved handling of the vehicle.The figure 1.2 shows the typical schematics of passive suspension.

1.2.3 Active Suspension System

Active suspension system is a recent derivation of the suspension technology. Active suspension system, possess the dedicated dynamic control component for opera-

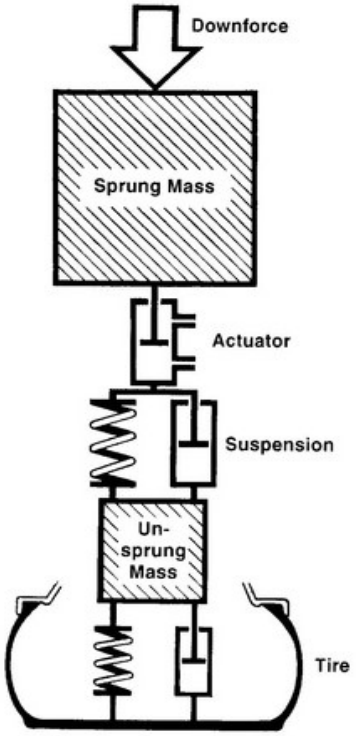

Fig. 1.2. Typical semi-active suspension schematics [22]

tion of suspension against the road roughness/ disturbance. Active suspension system requires constant power source, transmission mechanism for the generated force by power source, and sensory network and microcontroller for the control mode selection. Active suspension has capability to vary damping force required for the ride comfort against the road disturbances experienced by the vehicle. Multiple control mode operation to compensate for the variety of the road roughness facilitates improved vehicle handling performance, and thus achieves the better stability of the vehicle compared to passive and semi-active suspension systems. Also, cornering abilities are enhanced due to the reactive inertia applied against the spring deformation while turning [21]. The figure 1.3 shows the typical schematics of passive suspension.

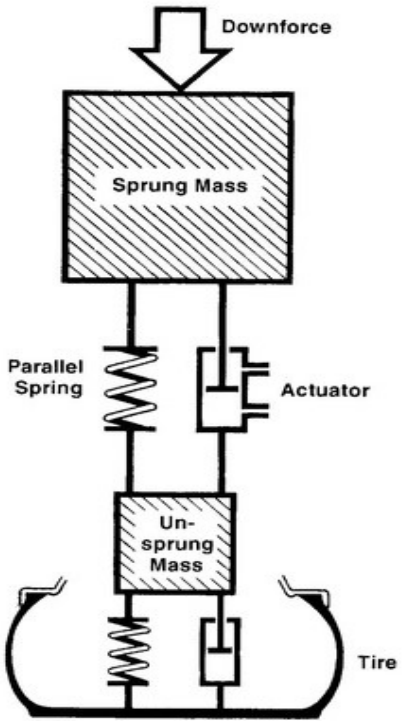

Fig. 1.3. Typical active suspension schematics [22]

1.3 Closure on the Chapter

This chapter summarizes the research objectives and major steps involved in the research. Also, chapter documents the overall suspension system types, and differentiating factors from each other. The vehicle performance implications are documented as well. This research focuses on active suspension with magneto-rheological damper being the force actuator. The electromagnetic activation of MR fluid generates necessary force for achieving the desired ride comfort and vehicle handling performance. Next chapter focuses on the mathematical modeling of passive suspension and active suspension with MR damper. Bingham, Dahl, and Bouc-Wen models are considered for the active suspension hysteresis design. The passive suspension system is modeled to serve as basis for active suspension model improvement comparison.

2. MATHEMATICAL MODELING OF PASSIVE AND ACTIVE SUSPENSION WITH HYSTERESIS

The most employed and useful model of a vehicle suspension is a quarter car model. Although, the quarter car model has no representations of the geometric effects of a full car model and offers no possibility of studying longitudinal and lateral interconnections, it contains the most basic features of the real problem and includes representation of the problem of controlling wheel and wheel-body variations. In this project, a quarter car model with passive and active suspension is designed for the performance analysis of MR suspension. The governing equations explained below are used to design the quarter car suspension model. Table 2.1 shows the quarter car parameters considered for the plant modeling.

Table 2.1.
Quarter car parameters used for the plant modeling

Parameters	**Value**
Sprung mass	2500 [Kg]
Unsprung mass	320 [Kg]
Suspension spring stiffness	80000 [N/m]
Tire stiffness	500000 [N/m]
Suspension damping coefficient	320 [Ns/m]
Tire damping coefficient	15020 [Ns/m]

2.1 Passive Suspension

The passive suspension system is a system in which the characteristics of the spring and the damper are fixed. The spring and damper characteristics are determined according to the goals and its intended application. Governing equations for the passive suspension are determined from the free body diagram of quarter car suspension physical model.

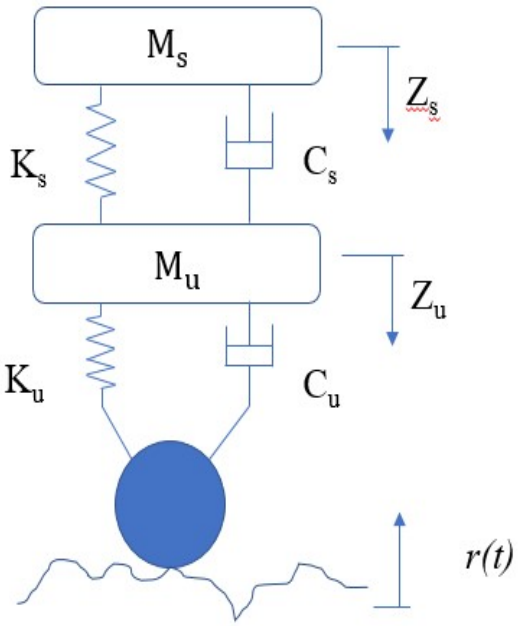

Fig. 2.1. Free body diagram of passive suspension quarter car model

Sprung mass dynamics for the passive suspension can be written from the free body diagram shown in figure 2.1 is given by equation (2.1).

$$m_s\ddot{z}_s + c_s(\dot{z}_s - \dot{z}_u) + k_s(z_s - z_u) = 0 \tag{2.1}$$

Rearranging the equation (2.1), we can find the acceleration of the sprung mass, which is given by equation (2.2).

$$\ddot{z}_s = -\frac{(c_s(\dot{z}_s - \dot{z}_u) + k_s(z_s - z_u))}{m_s} \tag{2.2}$$

Unsprung mass dynamics for the passive suspension can be written from the free body diagram shown in figure 2.1 is given by equation (2.3).

$$m_u\ddot{z}_u + c_s(\dot{z}_u - \dot{z}_s) + k_s(z_u - z_s) + c_u\dot{z}_u + k_u z_u = k_u r + c_u\dot{r} \tag{2.3}$$

Rearranging the equation (2.3), we can find the acceleration of the unsprung mass, which is given by equation (2.4).

$$\ddot{z}_u = \frac{k_u r + c_u\dot{r} - (c_s(\dot{z}_u - \dot{z}_s) + k_s(z_u - z_s) + c_u\dot{z}_u + k_u z_u)}{m_u} \tag{2.4}$$

2.2 Active Suspension

Active suspension system consists of a conventional spring and a controllable shock absorber or damper. The viscous damping coefficient of the damper can be controlled in real time which gives an advantage over the passive suspension systems. The present study focuses on MR damper. Governing equations for the active suspension are determined from the free body diagram of active quarter car suspension physical model. Sprung mass dynamics for the active suspension can be written from the free body diagram shown in figure 2.2 is giben by equation (2.5).

$$m_s\ddot{z}_s + c_s(\dot{z}_s - \dot{z}_u) + k_s(z_s - z_u) = U_c \tag{2.5}$$

Rearranging the equation (2.5), we can find the acceleration of the sprung mass, which is given by equation (2.6).

$$\ddot{z}_s = U_c - \frac{(c_s(\dot{z}_s - \dot{z}_u) + k_s(z_s - z_u))}{m_s} \tag{2.6}$$

Unsprung mass dynamics for the active suspension can be written from the free body diagram shown in figure 2.2 is given by equation (2.7).

$$m_u\ddot{z}_u + c_s(\dot{z}_u - \dot{z}_s) + k_s(z_u - z_s) + c_u\dot{z}_u + k_u z_u = -U_c + k_u r + c_u\dot{r} \tag{2.7}$$

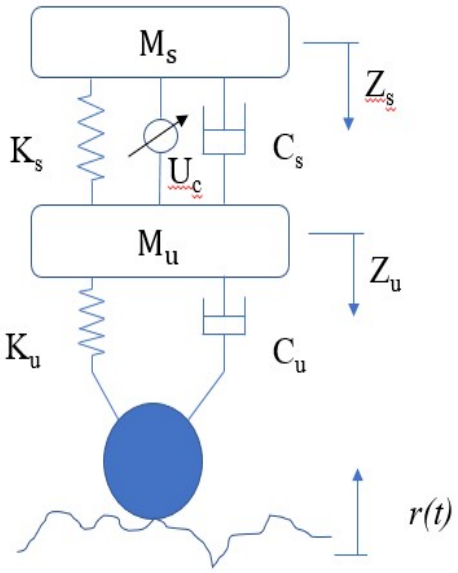

Fig. 2.2. Free body diagram of active suspension quarter car model

Rearranging the equation (2.7), we can find the acceleration of the unsprung mass, which is given by equation (2.8).

$$\ddot{z}_u = \frac{-U_c + k_u r + c_u \dot{r} - (c_s(\dot{z}_u - \dot{z}_s) + k_s(z_u - z_s) + c_u \dot{z}_u + k_u z_u)}{m_u} \tag{2.8}$$

In this research controlled damping force (Uc) is generated by using magento-rheological damper. Magnetorheological damper use the principle of electromagnetic induction for activation of MR fluid, and thus exhibit hysteresis behavior. MR damper and hysteresis modeling is discussed in the following subsections.

2.3 Magnetorheological Damper

Dissipation of energy by change in volume is the basic operating principle of dampers. As far the conventional dampers are considered dissipation energy due to road disturbances is function of the rate of change of volume flow rate caused by

damper piston orifice design and viscosity of the fluid. This operating principle makes conventional damper a constant energy dissipation damper.

Magneto rheological dampers have ability to change the viscosity of the fluid as a function of magnetic excitation provided to operating fluid. Increasing excitation results into the increased magnetic flux through the fluid, and thus the increased resistance to fluid flow, which results into increased dissipation of energy per cycle [21]. Based on the principle of construction, MR dampers are classified as single tube, twin tube, or double end dampers. Each type comes with its own advantages and disadvantages, the twin tube dampers are easier to manufacture and operate at lower pressures thus reducing the overall manufacturing and operation cost [21]. Monotube dampers on the other hand operate at higher pressures which results into low cavitation and thus more efficient operation of the damper. The gas accumulator also provides for a response time below 5 milliseconds which is a desirable characteristic when designing an active suspension [10]. Hence the best choice for an automotive damper per the construction consideration is monotube MR damper which is used in this research. Also, magneto rheological fluid and its properties affects the damper operation.

2.3.1 Magnetorheological Fluids

Magnetorheological fluids are smart fluids formed as a mixture of hydrocarbon oils and ferromagnetic particles, which exhibit change in physical properties when subjected to a magnetic excitation [21]. These fluids have gained wide popularity among the engineering world due to their applications in the automotive domain. MR fluids are characterized mainly by the concentration as well as the size and shape of the ferromagnetic nanoparticles suspended in the fluid [21]. Although the base fluids exhibit Newtonian behavior in the absence of a magnetic field, they can display Non-Newtonian behavior due to the effect of magnetism on the nanoparticles. By controlling the strength of the magnetic field, the shear strength of the MR fluid can

be altered, so that resistance to the MR flow can be varied [1].As discussed earlier, due to the dependency of MR fluid characteristics on the magnetic particle size, it is very hard to model a non-linear behavior of fluids with different compositions and hence the mathematical models for these fluids are established with linear relationship between the magnetic field strength and the magnetic flux density. The MR fluid display hysteretic behavior due to non-linear relationship between the magnetic flux and generated damping force [21]. The hysteresis in the MR suspension is an important phenomenon to simulate and study since the non-linear effects of hysteresis result in discontinuous relationship between the current in electromagnet and damping provided by the MR damper [23]. This research takes into consideration the hysteresis existed in the MR models. Bingham, Dahls, and Bouc-Wen models are modeled and simulated using the MATLAB/Simulink software package for the analysis of quarter car model with hysteresis loop in the simulation to identify the accurate response of the system for the various road profiles.

2.4 Hysteresis Models

Hysteresis is a phenomenon common to a broad spectrum of physical systems. As such, it is often present in plants for which controllers are being designed, where it introduces a nonlinear multi-valued behavior [23]. Three hysteresis models are considered in this research for MR damper active suspension modeling and simulation. The mathematical modeling of the hysteresis considering Bingham, Dahl, and Bou-Wen theory is explained in the following subsections.

2.4.1 Bingham Model of Hysteresis

The stress-strain behavior of the Bingham viscoplastic model (Shames and Cozzarelli, 1992) is often used to describe the behavior of MR (and ER) fluids. In this model, the plastic viscosity is defined as the slope of the measured shear stress versus

shear strain rate data. Thus, for positive values of the shear rate, , the total stress is given by equation (2.9)

$$\tau = \tau_{y(field)} + \eta\dot{\gamma} \tag{2.9}$$

Based on this model of the rheological behavior of ER fluids, Stanway, et al. (1985, 1987) proposed an idealized mechanical model, denoted the Bingham model, for the behavior of an ER damper. The Bingham model consists of a Coulomb friction element placed in parallel with a viscous damper. Bingham model is one of the initial models of the MR damper. Bingham plastic model behaves as solid till the minimum yield stress is reached, after the minimum yield stress point it follows the linear relationship between stress and the deformation. Bingham plastic model is proposed in 1985, and it can be formulated using equation (2.10) [7]:

$$F_{mr} = F_c * sgn(\dot{z}) + c_s\dot{z} + U_c \tag{2.10}$$

Signum (sgn) function takes care of direction of friction force Fc relative to the relative velocity of hysteresis variable z. Damping force (Fmr) is function of instantaneous vehicle velocity, viscous damping coefficient of MR fluid, when no electromagnetic excitation is provided to it. Uc is the variable and controllable damping force that can be generated according the particular fluid properties used as a damper fluid. Over the range of operation, Bingham model behaves nearly linear. Fluid properties used for the Bingham hysteresis model are as shown in Table 2.2.

Table 2.2.
Bingham hysteresis parameters for the plant modeling

Parameters	**Value**
Damping constant (C_0)	320 [Ns/m]
Offset force (F_0)	10 [N]
Friction force (F_c)	100 [N]

2.4.2 Dahl Model of Hysteresis

Dahl model of MR damper [8] considers the quasi-static bonds in the origin of friction [9]. Damping force (Fmr) is a function of instantaneous velocity of the damper piston. The damper piston velocity takes into account the road disturbance amplitude and acceleration vehicle is experiencing. Also, damping force considers hysteresis loop shape parameters (K, Kwa, Kwb,) and dynamic hysteresis coefficient (w). Dynamic hysteresis coefficient is determined at every instantaneous value of piston velocity and thus gives more robust hysteresis model as compared to Bingham model of hysteresis. The dahl model is formulated using equations (2.11) and (2.12)

$$F_{mr} = K\dot{z} + (K_{wa} + K_{wb}\nu)w \tag{2.11}$$

$$\dot{W} = \rho(\dot{z} - |\dot{z}|w) \tag{2.12}$$

Dahl hysteresis model parameters considered for the plant modeling are as shown in the table 2.3.

Table 2.3.
Dahl hysteresis parameters for the plant modeling

Parameters	**Value**
Control voltage (v)	5 [V]
Loop shape coefficient (K),	350
Loop shape coefficient (Kwa)	800
Loop shape coefficient (Kwb)	250
Loop shape coefficient ()	25

2.4.3 Bouc-Wen Model of Hysteresis

Bouc-Wen model takes into consideration the spring stiffness element, conventional damper, and the Bouc-Wen hysteresis loop elements [9, 24]. Bouc-Wen hysteresis is a function of road wave amplitude, instantaneous velocity, pre-yeild stress

of damper and MR fluid properties. Non-linear behavior of the yield stress and deformation is most accurately modeled in Bouc-Wen theory of hysteresis, and thus replicates the real time behavior of MR damper in the operational range. Bouc-Wen model is formulated using equation (2.13) [25]:

$$\dot{y} = -\gamma|\dot{z}|y|y|^{n-1} - \beta z|y|^n + A\dot{z} \tag{2.13}$$

is the evolutionary variable, which is dependent on , , and A. The nature of y changes from the sinusoidal to the quasi-rectangular function. The resulting force generated by the MR damper is calculated using the equation (2.14):

$$F_{mr} = C_s(u)\dot{z} + K_s z + \alpha(u)y + F_0 \tag{2.14}$$

Coefficients Cs(u) and α(u) are determined by the equations (2.15) – (2.16):

$$C_s(u) = C_{0a} + C_{0b}u \tag{2.15}$$

$$\alpha(u) = \alpha_{0a} + \alpha_{0b}u \tag{2.16}$$

Bouc-Wen hysteresis model parameters considered for the plant modeling are as shown in Table 2.4.

2.5 Closure on the Chapter

Chapter 2 summarizes types of suspension and the implication of the each on the ride comfort and vehicle handling performance of the vehicle. Also, mathematical modeling of quarter car passive suspension and active suspension for the plant modeling is well documented in this chapter. The superiority of MR damper over the conventional damper is highlighted in the discussion. MR damper hysteresis and non-linear behavior is explained using mathematical modeling considering Bingham, Dahl, and Bouc-Wen theory of hysteresis. Plant modeling is performed using the mathematical models describes in this chapter. MATLAB software package is used for the plant modeling of quarter car suspension system. The next section, chapter

Table 2.4.
Bouc-Wen hysteresis parameters for the plant modeling

Parameters	**Value**
Spring stiffness (K_0)	300 [N/m]
pre-yield stress of the damper (F_0)	0 [N]
γ	1
β	0
Road wave amplitude (A)	1.5
n	2
Control voltage (v)	5 [V]
C_0a	4400
C_0b	442
α_0a	10872
α_0b	49616
η	0

3 explains the road profiles considered for the simulation, significance of each road profile, and uncontrolled simulation responses.

3. ROAD PROFILES AND UNCONTROLLED (OPEN-LOOP) SYSTEM RESPONSES

3.1 Road Profiles

The road is the most intensive source of excitation of the vehicle. The vehicle vertical dynamic behavior (oscillations) depends on a series of factors, most of them related to the road: length, height, shape, irregularities frequency, etc. Every road has a profile of irregularities (small up and downs), which can be periodic or random (stochastic) [26]. Most of the real roads have a random profile or irregularities. Therefore, to study the suspension system behavior accurately research use six different road signals including road type C according to international standards ISO/TC108/SC2N67, which represent the real road profiles. These include; Step signal, sinusoidal signal, white noise, uniform random number input signal, mixed sinusoidal and uniform random number input signal, and road type C profile input.

3.1.1 Step Road Input

Step input signal is a basic input to simulate the response of the suspension system. It simulates a very intense force for a very short time, such as a vehicle drive through a speed hump. The suspension system simulation has been carried out for on-road as well as off-road conditions. The maximum excitation that a vehicle may undergo is during an off-roading activity. Therefore, 75 mm (0.075 m) step is considered for this project, which is the acceptable limit of displacement for an automotive suspension system [11]. Figure 3.1 shows the step road input considered for the simulation of the modeled suspension system.

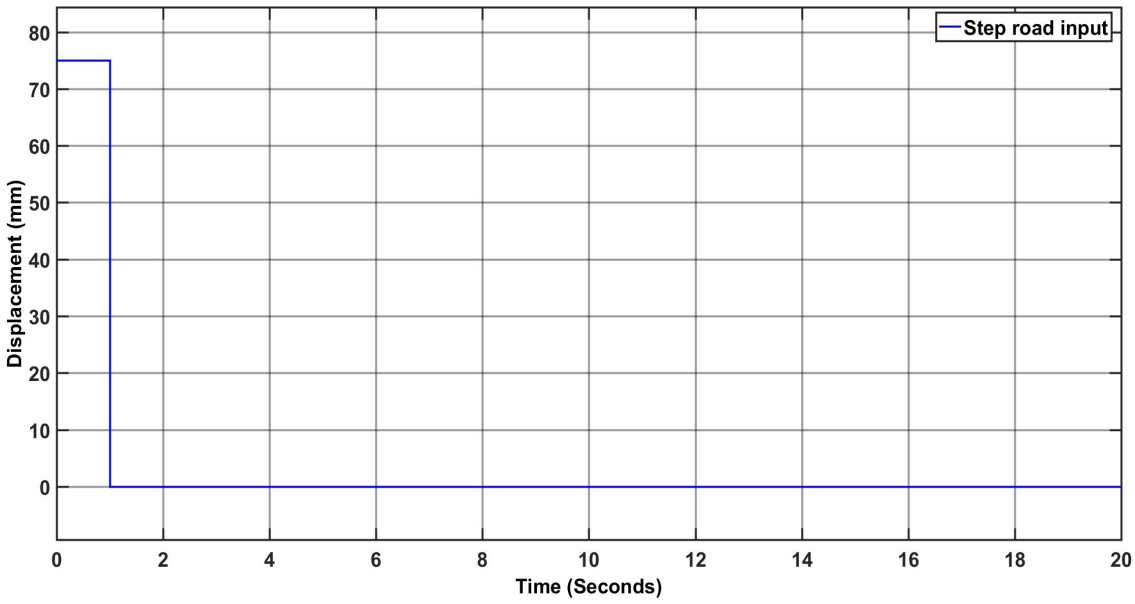

Fig. 3.1. Step road input for the plant model simulation

3.1.2 Sine Road Input

Sine wave input signal can be used to simulate periodic pavement fluctuations. It can test the vehicle suspension system elastic resilience ability while the car experiences a periodic wave pavement. Sine input pavement test is made by every automotive industry before a new vehicle drives on road [27]. Sine wave input of amplitude 75 mm (0.075 m) and frequency 20.8 rad/sec is given as road input [11]. Figure 3.2 shows the sine road input considered for the simulation of the modeled suspension system.

3.1.3 White Noise Road Input

Numerous researches show that when the vehicle speed is constant, the road roughness is a stochastic process which is subjected to Gauss distribution, and it cannot be described accurately by mathematical relations. The vehicle speed power spectral density is a constant, which corresponds with the definition and statistical character-

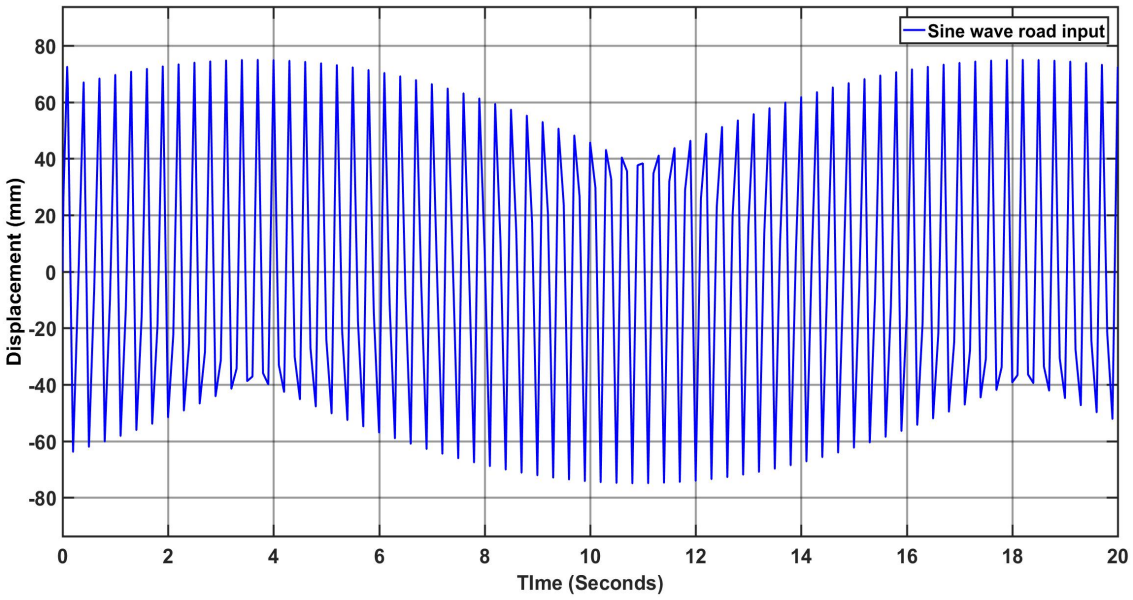

Fig. 3.2. Sine road input for the plant model simulation

istic of the white noise, so it can be simply transformed to the road roughness time domain model [11].

The transformation of white noise road input signal can perfectly simulate the actual pavement condition. It has a random character when it is used for the vehicle vibration input of road roughness. Figure 3.3 shows the white noise road input considered for the simulation of the modeled suspension system.

3.1.4 Uniform Random Number Road Input

There is no single definite method to analyze or synthesize the vibrations generated by a vehicle travelling over an irregular terrain. The apt method thus assumes that the vibrations can be approximated by a zero mean, normally distributed random (Gaussian) signal.

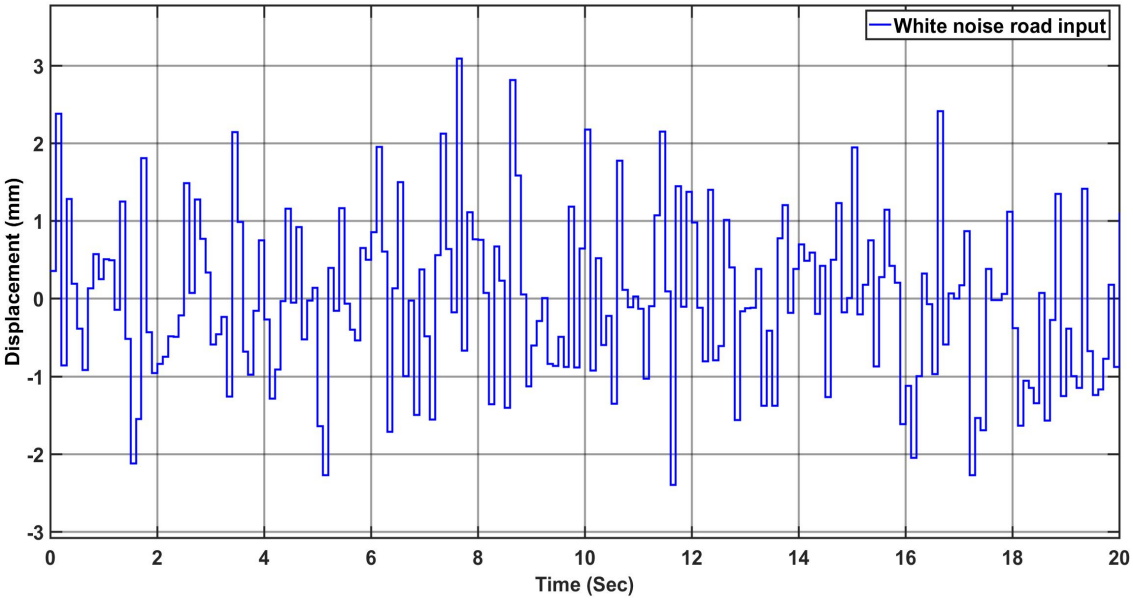

Fig. 3.3. White noise road input for the plant model simulation

The MR damper models are simulated using a standard uniform random number road profile with maximum and minimum boundaries of 75 and -75 respectively and 0.1s as a sampling time [11]. Figure 3.4 shows the uniform random number road input considered for the simulation of the modeled suspension system.

3.1.5 Mixed Road Input

This road profile is a combination of the wavy and rough road profile, which resembles the off-roading conditions. Sine wave input of a frequency 20.8 rad/sec and random number road profile with maximum and minimum boundaries of 75 and -75 respectively and 0.1 as a sampling time are coupled as the excitation from road to the wheel. Figure 3.5 shows the mixed road input considered for the simulation of the modeled suspension system [11].

Mixed road input resembles the uncertainties involved in the road disturbances experienced by the vehicle body. The modeled suspension system is tested against

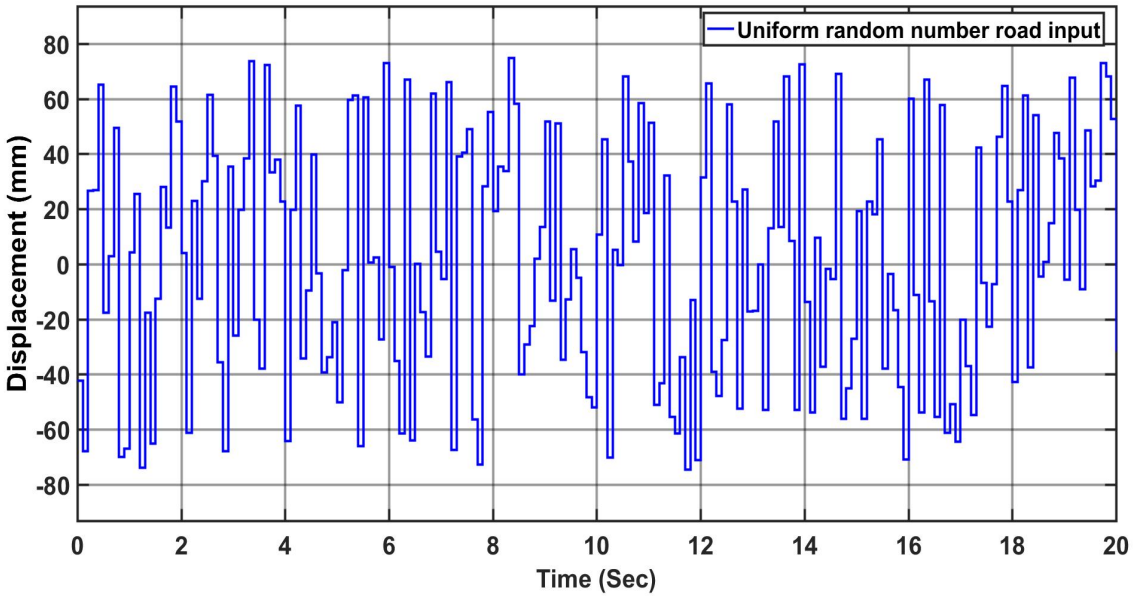

Fig. 3.4. Uniform random number road input for the plant model simulation

the road disturbance uncertainties to validate the feasibility of designed suspension system under unexpected conditions.

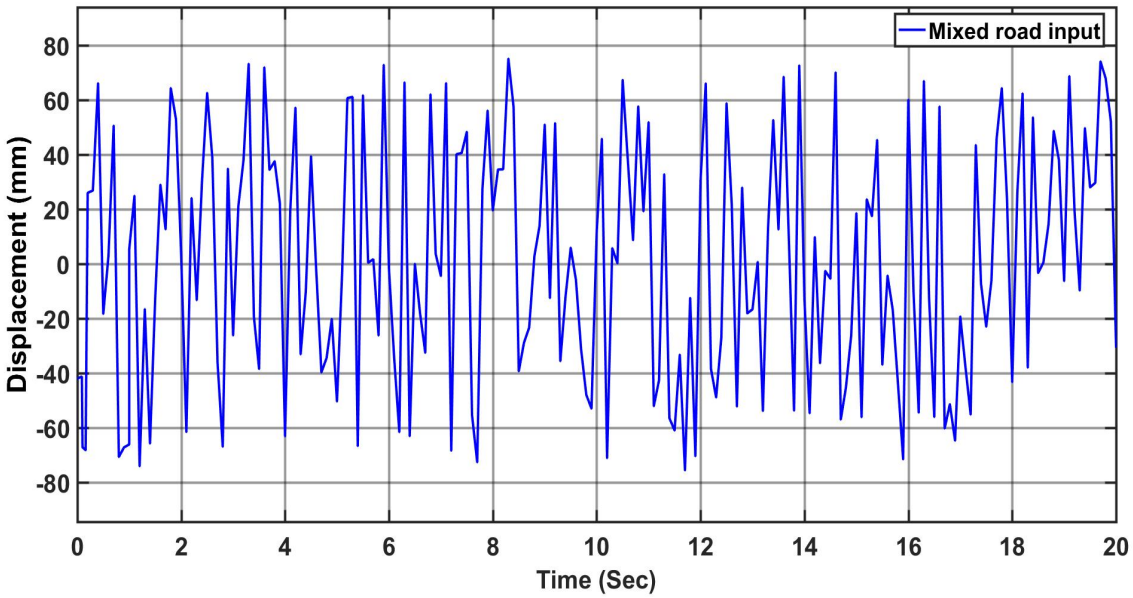

Fig. 3.5. Mixed road input for the plant model simulation

3.1.6 Road Type C Input

Road class C input is derived from the international standards ISO/TC108/SC2N67. International standards for the vertical power spectral density defines the road roughness. This transformation of white noise perfectly simulates actual road conditions. To derive this road profile, reference spatial frequency is considered as 0.1 per meter, frequency index as 2, and the vehicle speed as 45 mph. This derives the geometric average for the road profile definition. This road profile is a combination of all the above independently considered road profiles for the simulation [11]. Figure 3.6 shows the road type C input considered for the simulation of the modeled suspension system.

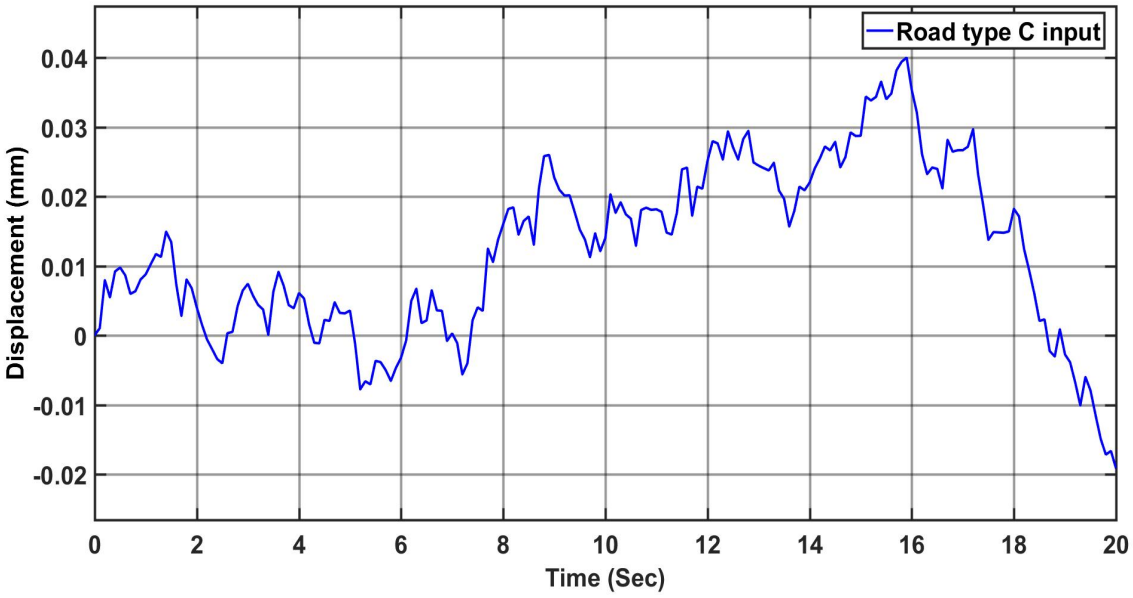

Fig. 3.6. Road type c input for the plant model simulation

3.2 Uncontrolled (Open-Loop) Simulation Responses

The passive suspension and semi-active suspension system with magneto-rheological controllable damper are modeled using the MATLAB/SIMULINK. MR damper is

designed considering the Bingham, Dahl, and Bouc-Wen with hysteresis. The developed hysteresis models are considered for the quarter car system design. The effect of the hysteresis model based on the overshoot and settling time is evaluated. Figures 3.7–3.17 shows comparative graphs for the sprung-mass displacement subject to step input, sine wave input, white noise input, random uniform number input, mixed road profile, and road class C derived from international standards ISO/TC108/SC2N67.

3.2.1 Open Loop Simulation Responses for Step Road Input

A road step input of 75 mm is used as road disturbance to the wheel [8]. The assumption is that all wheels experience the same road excitation. Figure 3.7 and figure 3.8 represents the response of each model in t erms of sprung mass displacement, and magnitude and phase change respectively for the given road profile. Figure 3.7 shows that Bouc-Wen model has minimum overshoot and the lowest settling time as compared to the other models. The step input simulates the sudden bump condition, which is a rare phenomenon for real operating conditions. Thus, consideration of settling time as well as overshoot is very important than just overshoot for this road profile. Bouc-Wen model has lowest overshoot and lowerst settling time for such conditions. Also, from Figure 3.8 it is observed that Bouc-Wen model goes through least phase changes until the vibrations are damped, which results into least hysteresis loss.

3.2.2 Open Loop Simulation Responses for Sine Road Input

Sine wave input of amplitude 75 mm and frequency of 20.8 rad/sec is given as road input [8]. The sine wave simulates the wavy road disturbance; simultaneous crest and trough profile of the road. Figures 3.9 and 3.10 represent the responses of each model in terms of sprung mass displacement, magnitude and phase change respectively for the sine road profile input. From figure 3.9 it is observed that the Bouc-Wen model has least overshoot as well as least sprung mass vertical displacement superposition,

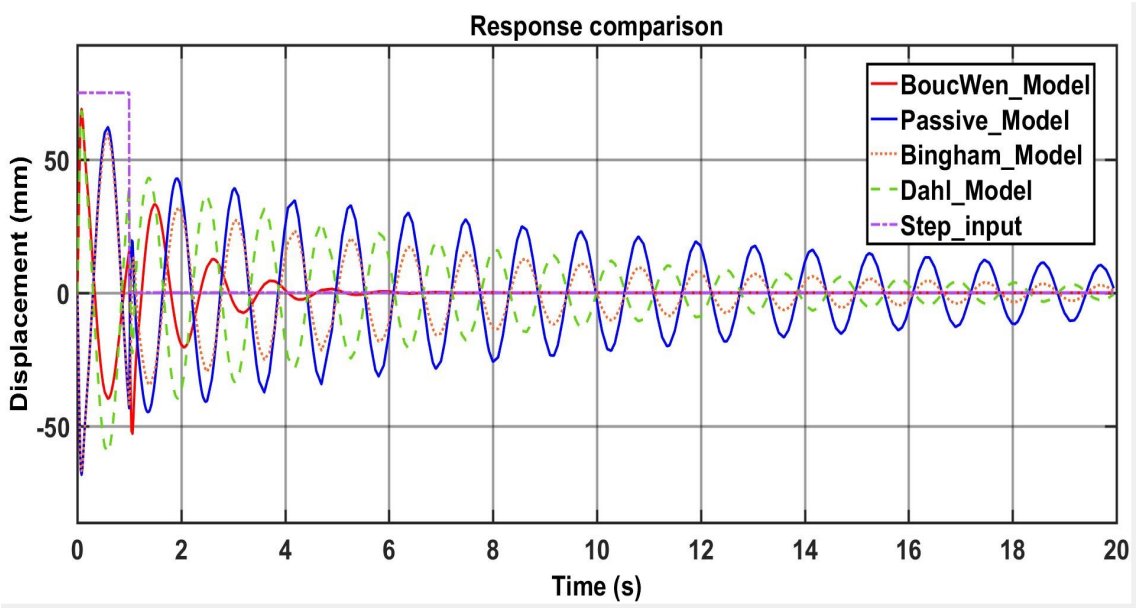

Fig. 3.7. Comparative response of all models for step road input

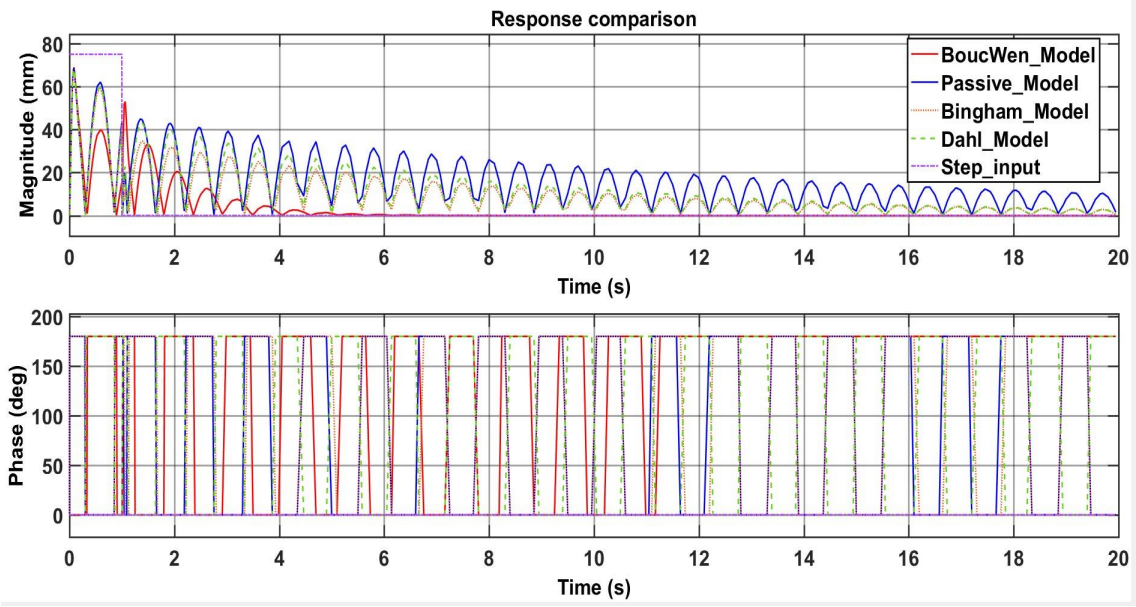

Fig. 3.8. Magnitude and phase analysis of all models for step road input

and hence results into the maximum comfort of passengers compared to other models. Figure 3.10 represents the magnitude of the displacement and signal phase change.

The Bouc-Wen model follows the road profile with lease vertical displacement of vehicle sprung mass.

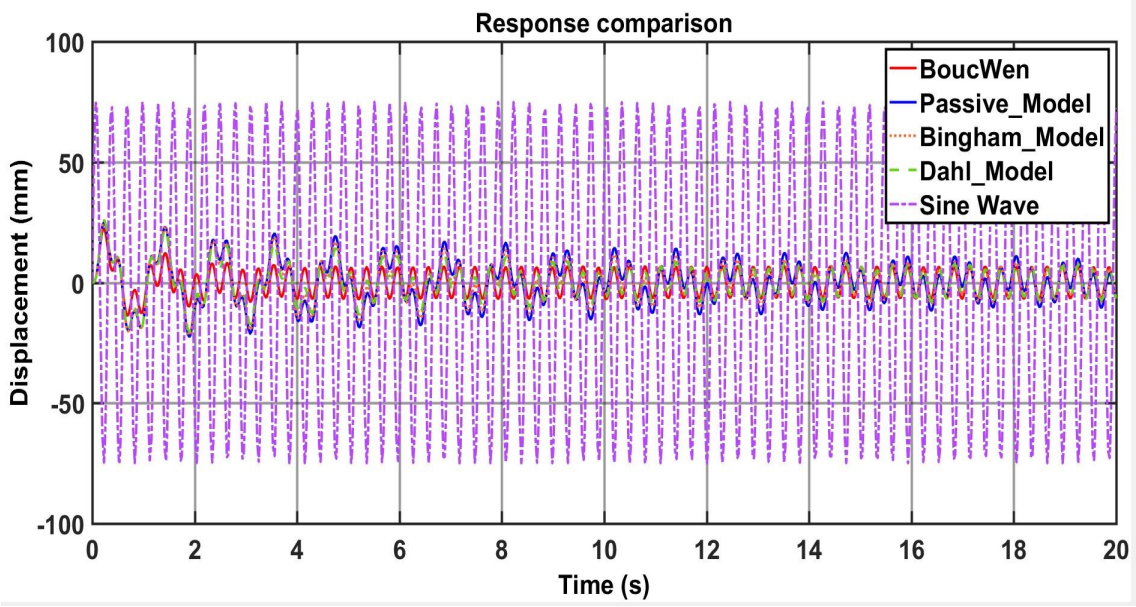

Fig. 3.9. Comparative response of all models for sine road input

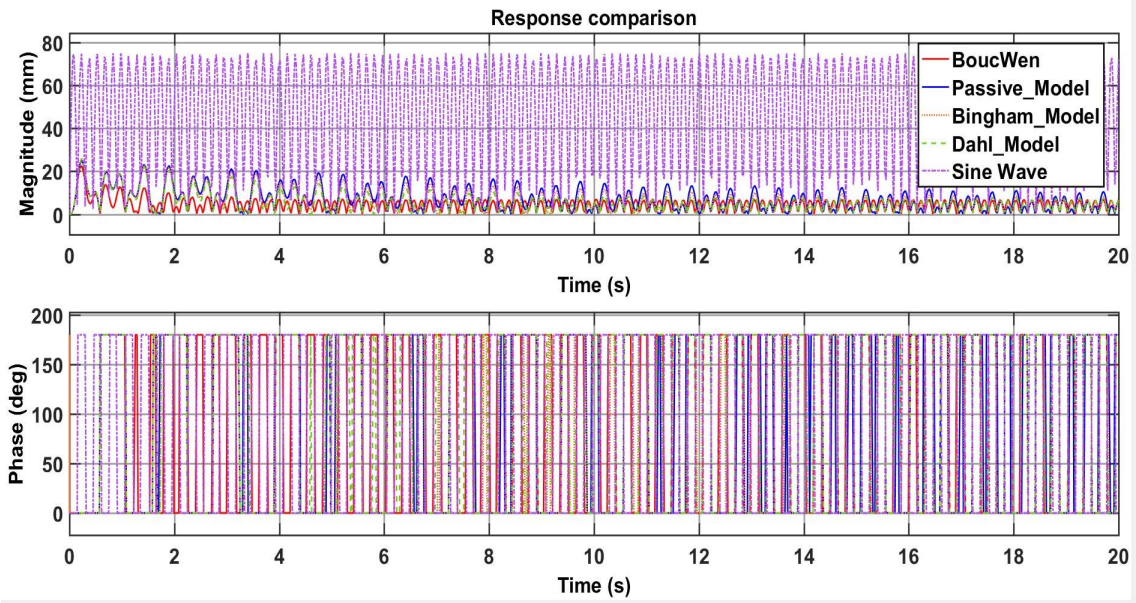

Fig. 3.10. Magnitude and phase analysis of all models for sine road input

3.2.3 Open Loop Simulation Response for White Noise Road Input

White noise is a random vibration signal with uniform intensity over the time with varying frequency which represents the road roughness variations for simulation. From the Figures 3.11 and 3.12, it is observed that the Bouc-Wen model has least overshoot and settling time compared to the remaining models. Figure 3.11 shows the vehicle sprung mass displacement and the phase changes for the Bouc-Wen model compared to the Dahl model, Bingham model, and passive suspension model. Thus, the Bouc-Wen model obtains the maximum comfort and minimum hysteresis loss.

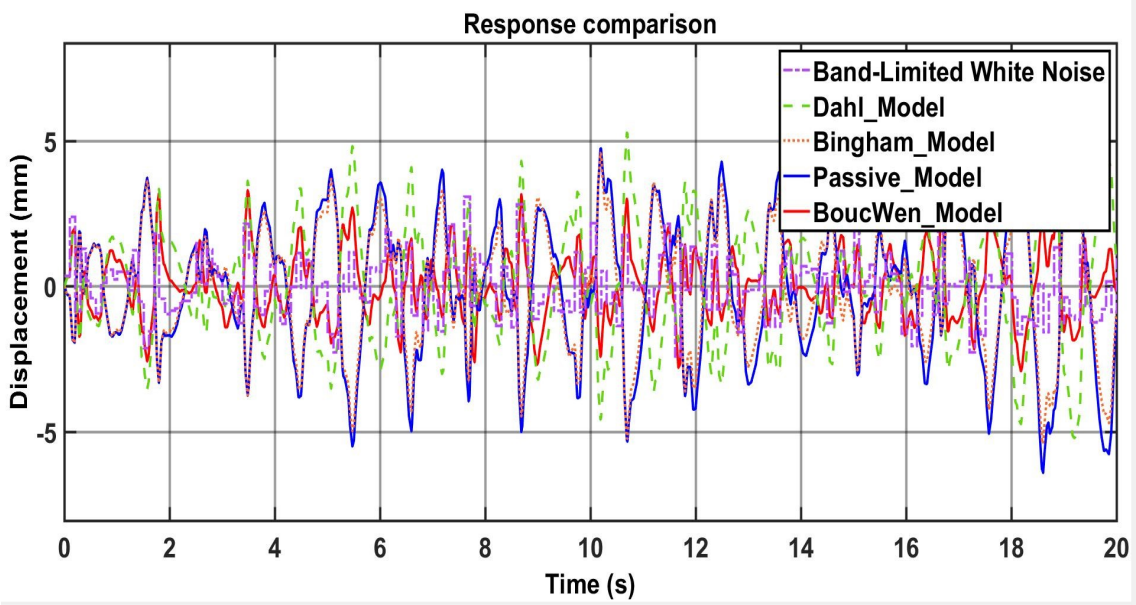

Fig. 3.11. Comparative response of all models for white noise road input

3.2.4 Open Loop Simulation Response for Uniform Random Number Road Input

There is no single definite method to analyze or synthesize the vibrations generated by a vehicle traveling over an irregular terrain. The apt method thus assumes that the vibrations can be approximated by a zero mean, normally distributed random

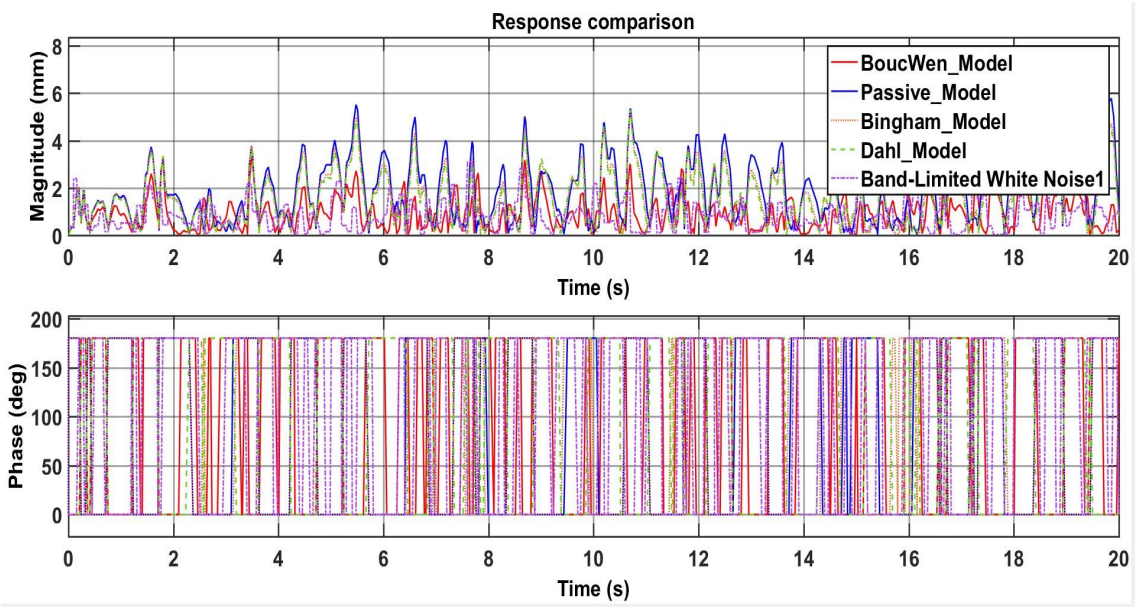

Fig. 3.12. Magnitude and phase analysis of all models for white noise road input

(Gaussian) signal [15]. Models are simulated using the uniform random number road profile with minimum and maximum bound -75 mm and 75 mm respectively. Figure 3.13 represents that the Bouc-Wen is most efficient model under such conditions, in turn provides the maximum ride comfort. Figure 3.14 shows the sprung mass displacement amplitude and phase change for the given road profile.

3.2.5 Open Loop Simulation Response for Mixed Road Input

This road profile is a combination of the wavy and rough road profile, which resembles with off-roading conditions. Sine wave input of amplitude 75 mm, frequency 20.8 rad/sec and random number road profile with minimum and maximum bound -75 and 75 respectively and 0.1 as a sampling time are couple as the excitation from road to wheel [8]. Figure 3.15 Shows that the Bouc-Wen model has least overshoot as well as settling time compared to the other models, thus provides the maximum ride comfort to the passengers. Figure 3.16 also helps to understand the sprung mass

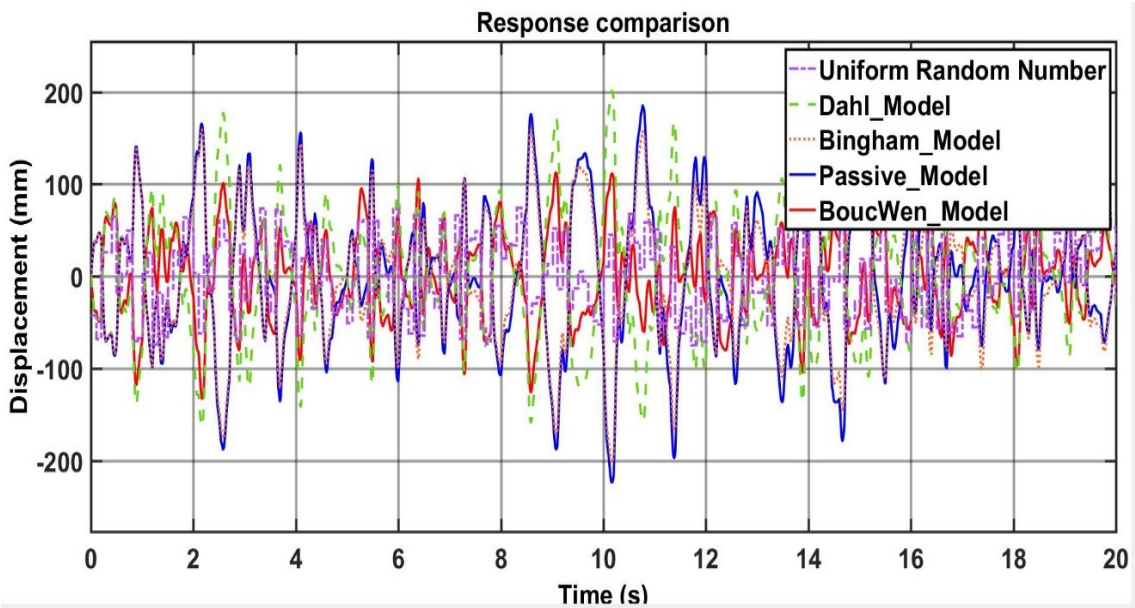

Fig. 3.13. Comparative response of all models for Uniform random number road input

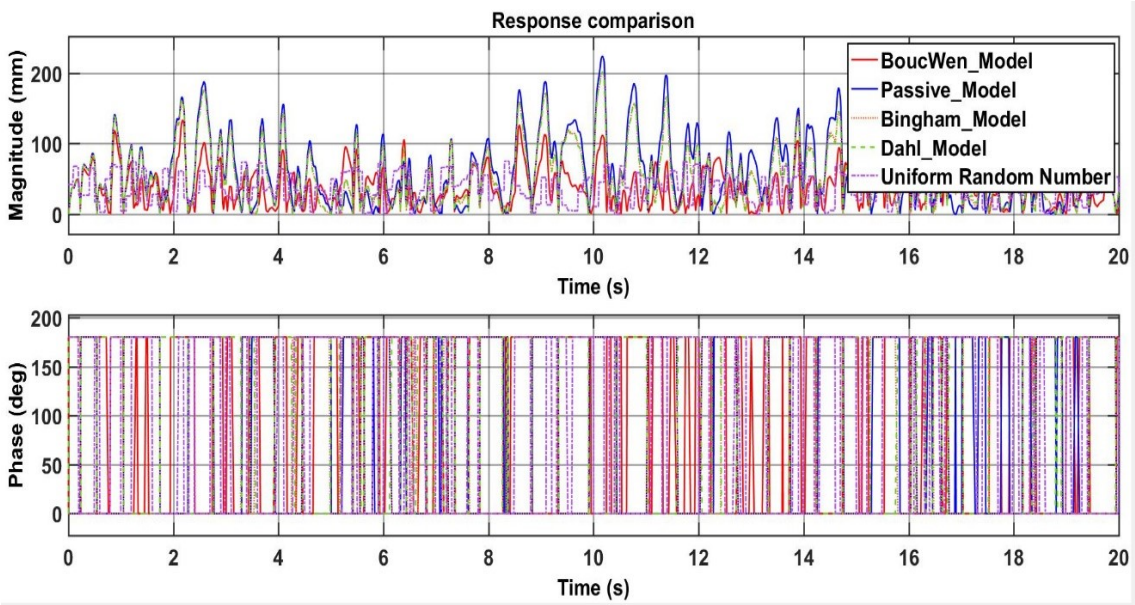

Fig. 3.14. Magnitude and phase analysis of all models for Uniform random number road input

displacement in vertical direction due to the road profile roughness, and the phase changes due to change in the road profile.

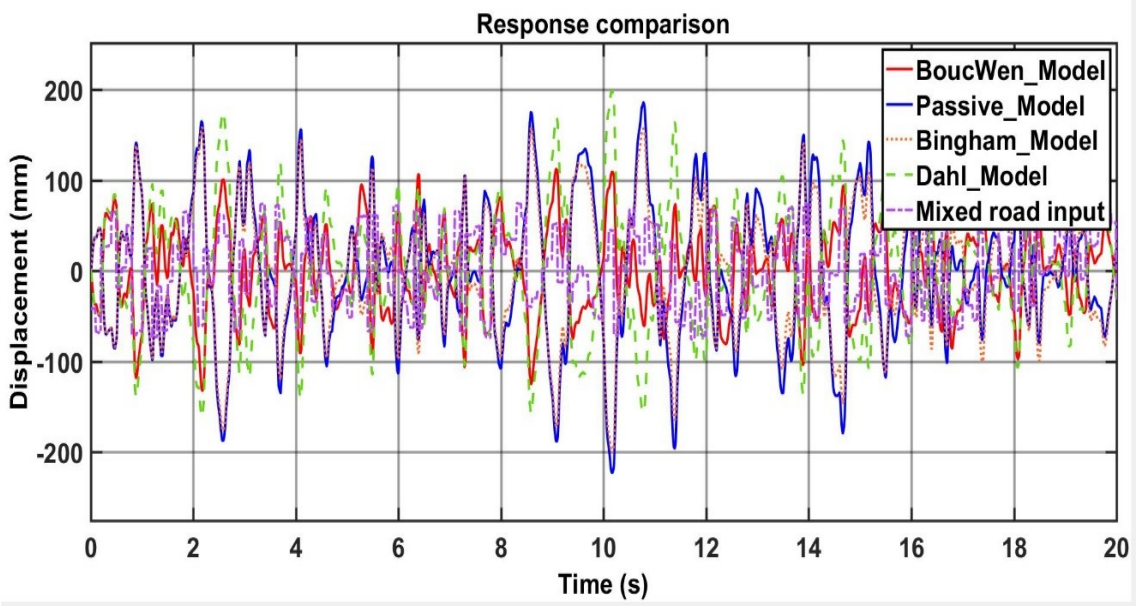

Fig. 3.15. Comparative response of all models for mixed road input

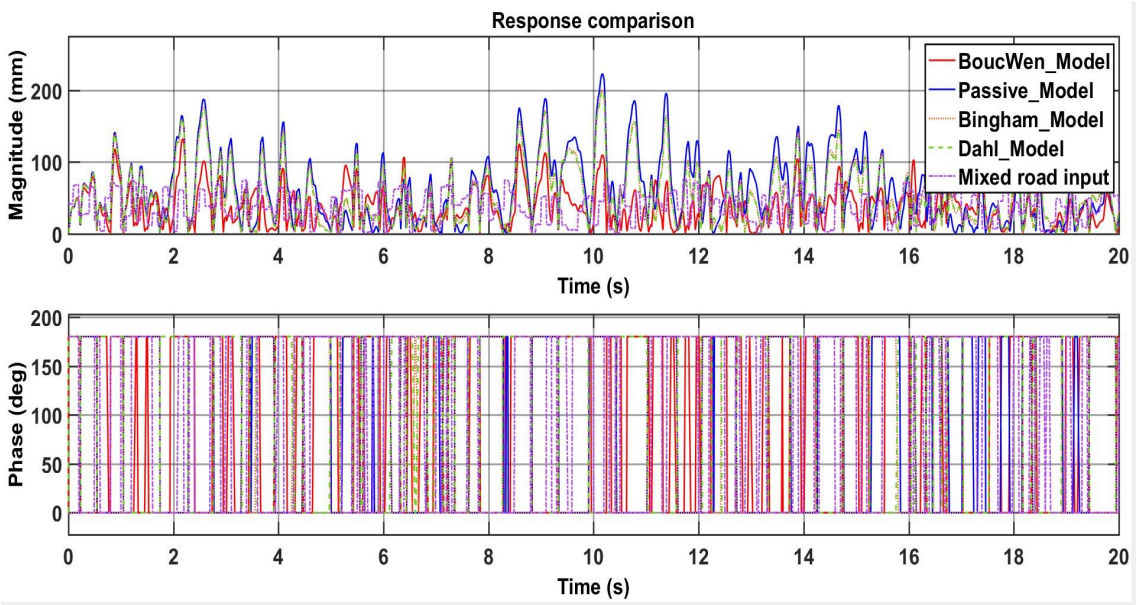

Fig. 3.16. Magnitude and phase analysis of all models for mixed road input

3.2.6 Open Loop Simulation Response for Road Type C Input

Road class C input is derived from the international standards ISO/TC108/SC2N67. International standards for the vertical power spectral density defines the road roughness. This transformation of white noise perfectly simulates actual road conditions. To derive this road profile, reference spatial frequency is considered as 0.1 per meter, frequency index as 2, and the vehicle speed as 45 mph. This derives the geometric average for the road profile definition. This road profile is a combination of all the above independently considered road profiles for the simulation [10]. The response obtained for all the four models is shown in the figure 3.17.

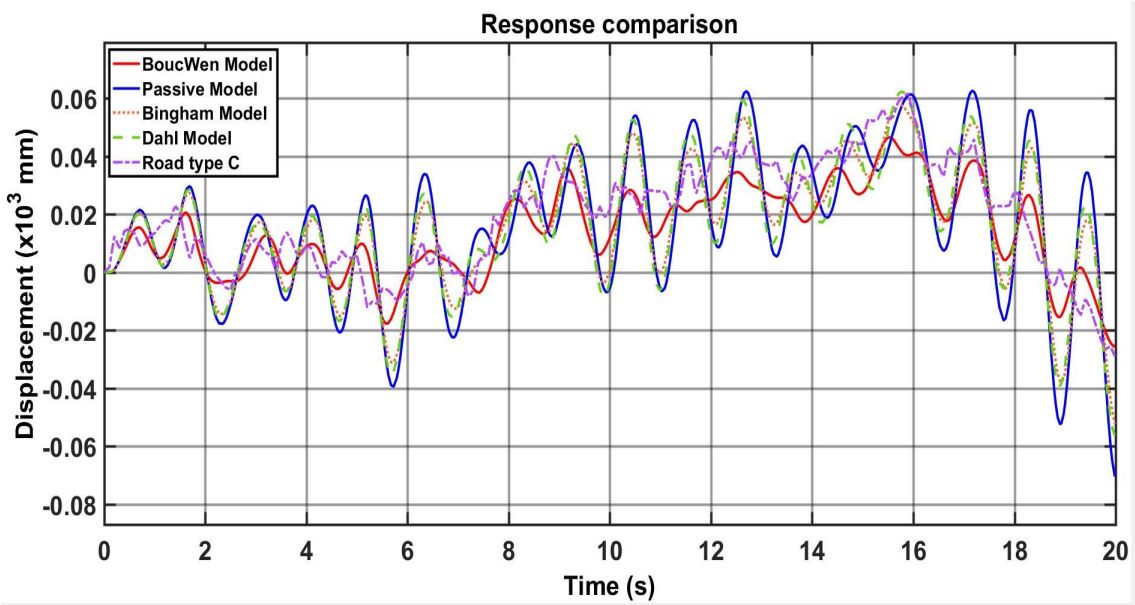

Fig. 3.17. Comparative response of all models for road type C input

Figure 3.17 shows that the Bouc-Wen model has least vertical vehicle body displacement as compared to passive, Bingham, and Dahl model. The least overshoot is observed with Bouc-Wen model, and thus results into the better ride comfort than other passive and active suspension models. Also, the improved vehicle handling performance can be viewed indirectly as the response of Bouc-Wen model adheres to the road disturbances.

3.3 Damping Force Determination for Bouc-Wen Suspension Model

The analysis of the models has been performed for the various road profiles as discussed above. The Bouc-Wen model shows the most efficient and optimum results with least overshoot and less settling time for the sine wave input, white noise input, uniform random number input, and the mixed sine wave and uniform random number input. The road profiles considered for the simulation and analysis simulates real time operating conditions. For the above stated reason Bouc-Wen model is considered for the MR damper design. The damping force requirement analysis is performed for the Bouc-Wen with the maximum disturbance of the road profile. Figure 3.18 shows the damping force requirement for the maximum disturbance of 75 mm. The peak finder analysis shows that the maximum damping force requirement for the damper is 2003 N as mentioned in the table 3.1. Considering the factor of safety in unexpected conditions, damper is designed and geometrically optimized for the force of 2150 N. Damper design and optimization is explained in chapter 4.

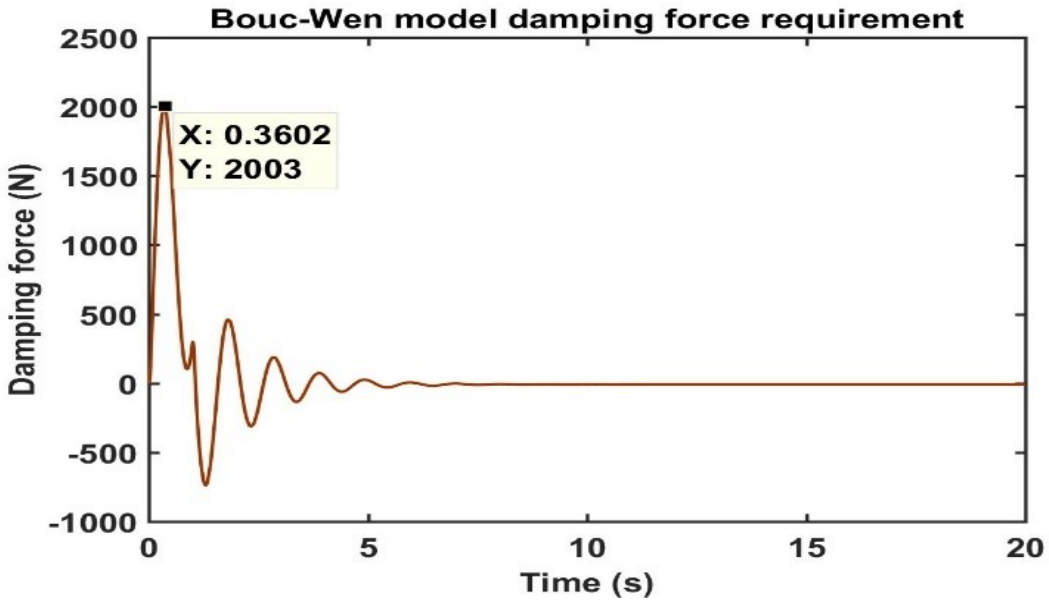

Fig. 3.18. Time Vs Damping force requirement for Bouc-Wen model

Table 3.1.
Bouc-Wen model damping force requirement statistics

	Value (Newton)	**Time (Seconds)**
Max	2003	0.3602
Min	-946.8	1.2391
Peak to peak	2953	
Mean	74.30	
Median	-8.005	
RMS	341.3	

3.4 Closure on the Chapter

Chapter 3 Summarizes road profiles considered for the simulation of modeled suspension system. Open loop responses of all models without any controller implementation are analyzed for road profiles explained in the section 3.1. In the conclusion, it has been observed that the Bouc-Wen suspension model experiences the less overshoot and minimum settling time. This behavior of Bouc-Wen encourages the further study on the MR damper using Bouc-Wen hysteresis. Design, mathematical modeling, and multi objective optimization is explained in the next chapter.

4. MR DAMPER ANALYTICAL CALCULATIONS, DESIGN OPTIMIZATION, AND SENSITIVITY ANALYSIS

4.1 MR Damper Geometry

MR damper works on the principle of electromagnetic induction. The magnetic flux lines passing through the MR fluid passage determines the instantaneous viscosity of MR fluid, and thus damping force generated by damper. Besides the activation current through a coil, geometric parameters also determine damping force provided by MR damper. Geometrical parameters differs in sensitivity towards the damping force change due to change in particular parameter. The following discussion concludes the effect of geometrical parameters on damping force provided by MR damper. The primary factors affecting the damping force are damper geometry, inductive current and the MR fluid characteristics [1]. The Pole Length (L), Piston Radius (R), and gap thickness (g) are the dominant geometrical parameters whereas the current through the coil and piston velocity are the non-geometric factors. Figure 4.1 shows a typical damper cross sectional view and the magnetic links of the circuit in the MR damper. From figure 4.1 and basic concepts of fluid mechanics, each parameter and its effect on the damping force can be evaluated as described further.

The viscous damping force is directly proportional to the piston radius which is a function of fluid flow resistance. The current dependent damping force is also directly proportional to the piston radius as the increase in piston radius increases the coil width which eventually means more current passing through the coil. Gap thickness also affects both, the viscous and current dependent damping force. It is the only parameter which varies inversely with respect to the damping force, i.e. wider the gap, less is the damping force as the magnetic flux density is less in a wider gap as

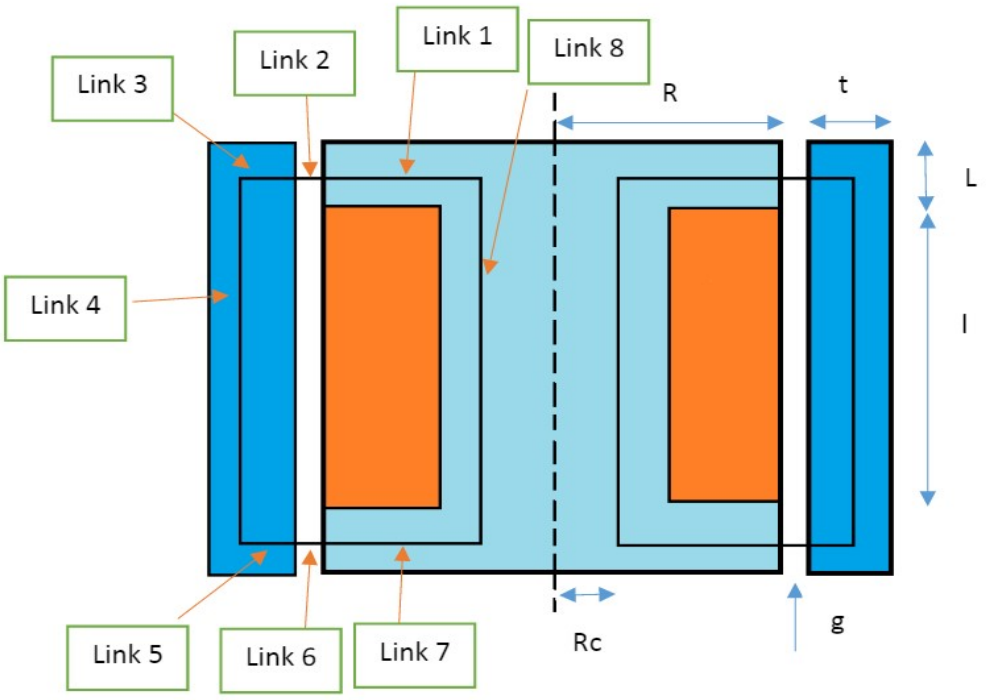

Fig. 4.1. Magneto rheological damper cross sectional view

fluid provides a high reluctance in the magnetic circuit. Wide gap also allows for easier flow of the fluid from the top of the piston to its bottom which reduces the viscous damping force due to the decrease in resistance to the flow. Pole length is a parameter which only affects the current dependent damping force. Pole length is normal to the axial flow direction, and shear resistance due to geometry is negligible. However, the greater the pole length, greater the area available for magnetic flux lines to pass through the circuit. Coil current is the most important variable for the MR damper design since the current dependent damping force varies exponentially with a change in coil current. This is due to the nonlinear increase in shear stress with a linear increase in the magnetic field strength. Piston velocity is another critical parameter in design of a damper. Viscous damping force is proportional to the piston velocity, thus as velocity increases, the current needs to be reduced to adjust the resultant damping force. The maximum piston velocity occurs at the instant the vehicle undergoes

a bump with maximum amplitude. Knowing the effect of considered geometrical parameters, sensitivity analysis is performed. The sensitivity analysis determines each parameter sensitivity within allowable range to provide maximum damping force against the road disturbance. Section 4.2 explains the sensitivity analysis in detail.

4.2 Sensitivity Analysis

Sensitivity analysis is performed for the dominant geometrical parameters such as piston radius, piston core radius, pole length, gap thickness, and cylinder thickness to determine the sensitivity order for optimization. The sensitivity analysis is performed at extreme operating conditions, which are no activation state (I=0Amp) and full activation state (I=2Amp) of MR damper. In the inactive state of damper, the current passing through electromagnetic coil is zero and damper should provide a viscous damping force of 726 N and a tolerance of 5 percent is considered for the sensitivity analysis. Figures 4.2 and 4.3 represents the sensitivity of all the parameters, at a coil current of 0A and 2A respectively.

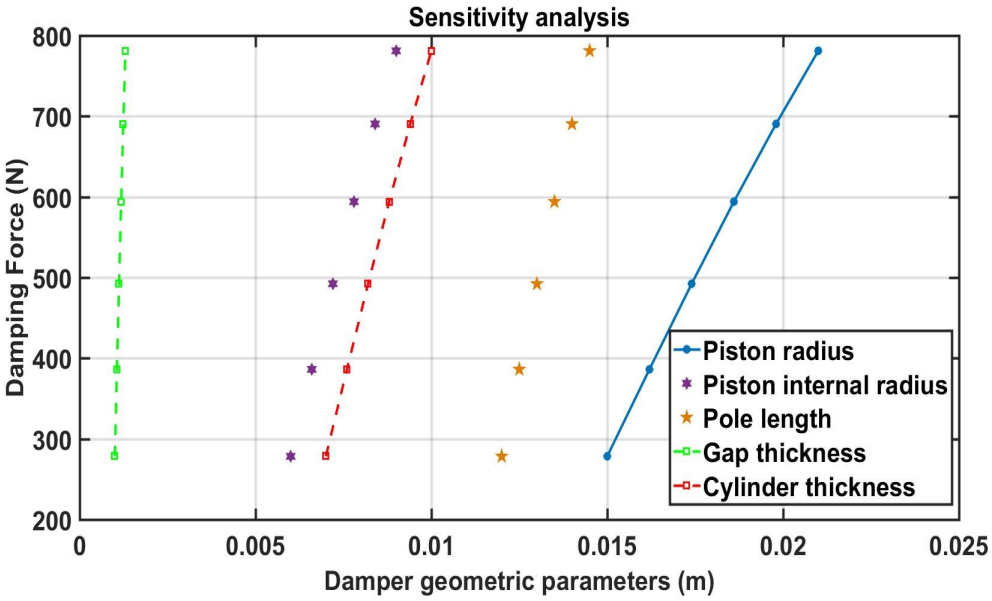

Fig. 4.2. Sensitivity analysis at no activation state (I=0Amp)

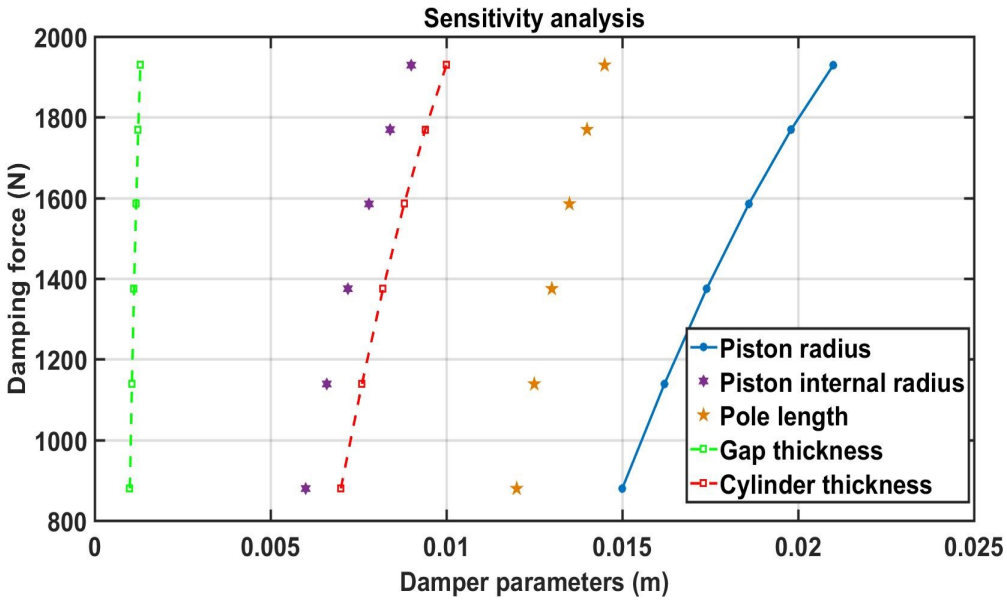

Fig. 4.3. Sensitivity analysis at no activation state (I=2Amp)

Figure 4.2–4.3 shows the sensitivity of critical geometric parameters considered subjected to damping force change. In both the boundary conditions, it has been observed that gap thickness is the most sensitive parameter towards the change in damping force provided by MR damper, and thus small change in gap thickness varies the damping force significantly. A sensitivity analysis was performed for the design variables and the effect of change in parameters on damping force is observed. As discussed in the above section critical parameters for the damping force determination of the MR damper are piston radius, pole length, gap thickness, cylinder thickness, and piston internal radius. The relationship between the parametric changes in each of the parameter on the damping force can be observed in the following graph. The highest the slope of the curve higher is the sensitivity and thus it can be observed in the figure 4.2 and figure 4.3, gap thickness has highest slope among the all parameters and thus it is the most sensitive parameter for the MR damper design. equation (4.1) used for the slope calculation.

$$Gap\_thickness\_slope = \frac{Y2 - Y1}{X2 - X1} \tag{4.1}$$

Δg=((1585-1375))/((0.00118-0.00112))

Δg = 3500000 N/m= 3500N/mm

Sensitivity analysis id very important for the optimization goal decision to vary a parameter with the given bounds (Constraints). Calculations of the slope as well as visually it is observed that gap thickness id the most critical factor while optimizing the MR damper parameters for the desired results.

4.3 Analytical Calculations for MR Damper Design

The analytical calculations part is the most critical phase of the design process as MR damper working is defined in terms of mathematical equations. This process involved the determination of spring force from the spring rate. The spring rate was calculated for general values of quarter car mass, motion ratio of the vehicle, desired spring frequency and the damping ratio range. The inputs for these values were selected for passenger car conditions from the OptimumG vehicle dynamics data [28]. Using these values, the spring force was determined and based on the spring force and the damping ratio limits, the damping force range requirement was obtained. This defined the constraints of our problem and then the five critical parameters were selected [1,2,5]. Further the road conditions were defined for the problem which will be discussed in detail further. The current range was specified between 0A to 2A, which is commercially acceptable limit obtained from the previous researches in the field. The MR fluid MRF-132EG from Lord Corporation is selected for the appropriate application [6]. The damper is designed to operate within the damping force range of 726N to 2150N, which is derived from the damping force analysis shown in figure 3.18 and table 3.1. The analytical design of the MR damper involves identification of important geometric parameters, using mathematical calculations and appropriate fluid flow equations through the damper body to define the operating range of the damping force. A Quasi-static quarter car model of the damper formulation involves determination of the spring force from basics of vehicle dynamics for desirable ride

frequencies of vibration of the sprung mass. This is based on various factors such as the type of vehicle for which the suspension is being designed, terrains for which the suspension is being designed i.e. highways or off-roading. The frequency of vibration for a vehicle being driven mostly on off-road terrains should be around 0.7 Hz and that for a regular car being driven on smooth roads is 1.6 Hz [16]. To facilitate a smooth operation under both conditions the frequency adapted in this study is 1.2Hz [28]. Considering the commercially available suspension springs and suitability for the application intended in a research, motion ratio and spring stiffness are the most important derived factors. The basic spring characteristics for damper design can be obtained using equations (4.2) – (4.3) [10].

$$f_s(Hz) = \frac{1}{2\pi M_R}\sqrt{\frac{K_s}{M_s}} \tag{4.2}$$

$$K_s = 4\pi^2 f_s^2 M_s M_r^2 \tag{4.3}$$

For a passenger car, a feasible spring length is 15 inches and the allowable deflection for smooth operation is 4.5 inches [28]. Based on the requirements, the maximum allowable force acting on the spring can be determined using equations (4.4) – (4.5).

$$F_{max} = K_s(Length_{free} - Length_{deflected}) \tag{4.4}$$

$$F_{max} = K_s(MaximumDeflection) \tag{4.5}$$

Using equations (4.2) – (4.5), for passenger car, the spring force is obtained to be 3306N. This value is in the acceptable range of 3000 4500N [16]. Further, an automotive suspension system is required to be underdamped for the smooth transition of vibrations with minimal shock to the passenger [10]. A critically and overdamped system will quickly reduce the sprung mass displacement magnitude but that will result into a jerk to the passenger. Considering an underdamped system, the damping force range is calculated for various operating conditions from the spring

force using the minimum and maximum damping conditions or damping ratios. The limits on damping ratios (min and max) used is between 0.25 and 0.65, where 0.25 is for an off-road terrain where minimum damping is desirable for a greater force transmissibility from ground to the sprung mass for a smoother ride [16]. Thus, the desired damping forces are 726 N to 2150 N using equations (4.6) – (4.7) [10].

$$DampingForce_{min} = \zeta_{min} * F_{max} \tag{4.6}$$

$$DampingForce_{max} = \zeta_{max} * F_{max} \tag{4.7}$$

Thus, the damper needs to generate a minimum force of 726 N, when there is no magnetic excitation of the MR fluid and the damping force is a function of the viscosity of the MR fluid and the piston velocity. Conversely, the damper needs to generate a maximum force of 2150N when the MR fluid is excited using electromagnetic induction. The MR fluid considered for this study is MRF-132EG [1,6] which is the common fluid used for automobile applications due to its low apparent viscosity when the fluid is not electromagnetically excited. The maximum piston velocity is derived from the desired spring stiffness, the road input, and ride frequency.

Road disturbances can be of any form, including sinusoidal, triangle, rectangular periodic waves, or a random combination of all the disturbances. However, all these signals can be modelled as a homogenous sinusoidal signal using Fourier and Laplace approximations [10]. The maximum disturbance producing sine wave input for the vehicle is considered for this model and the maximum piston displacement is set equal to the maximum spring deflection [10]. To determine the velocity, the road bump amplitude is modelled to be between 5cm to 10cm [8]. Using the equations (4.8) – (4.10) for harmonic motion for a road amplitude of 7cm and the frequency of 1.2 Hz, the maximum piston velocity is determined to be 0.5 m/s.

$$x(t) = A * cos(2\pi f_r t) \tag{4.8}$$

$$\dot{x}(t) = -A * 2\pi f_r sin(2\pi f_r t) \tag{4.9}$$

$$|Velocity_{max}| = |\dot{x}(t)_{max}| = A * 2\pi f_r \tag{4.10}$$

The lengths of magnetic links (L1-L8) are calculated from the geometry shown in figure 4.1 and subsequently the cross-sectional areas (A1-A8) of the links are calculated. Lengths of the link are given by equation (4.11) – (4.14).

$$L1 = L7 = R - \frac{R_c}{2} \tag{4.11}$$

$$L2 = L6 = g \tag{4.12}$$

$$L3 = L5 = \frac{t}{2} \tag{4.13}$$

$$L4 = L8 = 2L + z \tag{4.14}$$

Equation (4.15) – (4.22) determines the areas of links.

$$A1 = 2\pi L\big(R - \frac{R_c}{4}\big) \tag{4.15}$$

$$A2 = 2\pi L\big(R + \frac{g}{2}\big) \tag{4.16}$$

$$A3 = 2\pi L\big(R + g + \frac{t}{4}\big) \tag{4.17}$$

$$A4 = \pi((R + g + t) + (R + g + \frac{t}{4})^2) \tag{4.18}$$

$$A5 = 2\pi L\big(R + g + \frac{t}{4}\big) \tag{4.19}$$

$$A6 = 2\pi L\big(R + \frac{g}{2}\big) \tag{4.20}$$

$$A7 = 2\pi L\big(R - \frac{R_c}{4}\big) \tag{4.21}$$

$$A8 = \pi R_c^2 \tag{4.22}$$

Using equation (4.23), the total magnetic reluctance of the magnetic circuit is calculated.

$$(M_t) = \sum_{1}^{8} \frac{Li}{\mu i * Ai} \tag{4.23}$$

Where, μ2,6 = μmr and 1,3,4,5,7,8 = μs.

The relative permeability for MRF-122EG fluid is 5.5 and that of steel is 1600 [6]. Using equation (4.24), the magnetic flux (ϕ) in the circuit is further calculated [1]. .

$$\big(\phi\big) = \frac{N_c * I}{M_t} \tag{4.24}$$

Using equation (4.25), the magnetic flux density (B) in the circuit is calculated as 1.3039 Tesla for a current of 2 A [1]. The term $\mu 0$ refers to the permeability of vacuum.

$$\big(B\big) = \frac{\mu_0 * \phi}{A_2} \tag{4.25}$$

Since the magnetic flux density in the flow gap primarily contributes to damping force changes, only the flux generated in the gap is considered for damping force calculation. The flux density in the steel components does not contribute towards shear stress for development of the damping force and hence can be neglected. Using equations (4.26) – (4.27), the flow rate is calculated from the piston velocity and the piston shaft area [1].

$$\big(A_p\big) = \pi * [R^2 + \frac{R_c^2}{4}] \tag{4.26}$$

$$(Q)(\frac{m^3}{s}) = A_p * \dot{x}_p \tag{4.27}$$

The shear stress in the damper is determined using the equation (4.28) and MRF-122EG fluid datasheet [6].

$$\tau_y(kPa) = C_1 + C_2 * B + C_3 * B^2 + C_4 * B^3 \tag{4.28}$$

The viscous and current dependent damping force components (Fv) and (F) respectively, are determined using equation (4.29) – (4.31) [1]. Finally, the total damping force is determined using equation 45.

$$\big(F_\nu\big) = [1 + \frac{w_g * \dot{x}_p}{2Q}]\frac{12\mu Q(2L + z) * A_p}{w * g^3} \tag{4.29}$$

$$\left(F_{\tau}\right) = [2 + \frac{12Q\mu}{12Q\mu + 0.4wg^3\tau_y}]\frac{\tau_y L A_p sgn(\dot{x})}{g} \tag{4.30}$$

$$(F_{mr}) = F_{\nu} + F_{\tau} \tag{4.31}$$

Equations (4.1) – (4.31) defines the MR damper design. The multi objective optimization is performed to obtain the optimal values of piston radius, piston core radius, pole length, gap thickness, cylinder thickness. All the above mentioned parameters are calculated based on the optimized values determined using the optimization technique. The optimized values of the dominant geometrical parameters under consideration and calculated MR damper design parameters documented in the following section of the chapter.

4.4 MR Damper Geometric Optimization

To optimize output damping force, an integrated computation approach is used for each critical design parameter. The total damping force is defined as the objective function with damping force maximization criterion subjected to bounds on critical design parameters. The initial values of these parameters were adopted from the calculations and literature review [1,6,21]. The parameters in the constraint function are assigned minimum and maximum bounds for the generation of desired total damping force in the range of 826-2150 N which is calculated in the analytical model.

The optimization process incorporates the use of the pattern search methodology to determine the best possible values of parameters which satisfies the damping force conditions for minimum and maximum values of current through the coil. Pattern search method of optimization is useful for optimizing discrete functions which is desirable for the MR damper analysis.

The optimization is performed to maximize the damping force given by equation (4.32) – (4.33) constrained by inequalities given by equation (4.34).

$$(F_d) = f(R, g, L, t, R_c) \tag{4.32}$$

$$a_1 \frac{F_{mr}}{F_t} + a_2 \frac{\tau_d}{\tau_y} + a_3 \frac{D_{max}}{D_t} \tag{4.33}$$

Subject to:

$$0 < B < B_{max}, 0 < I < I_{max}, G_{min} < G < G_{max} \tag{4.34}$$

The total damping force (Fmr), shear stress (τ) and dynamic force range (D) are constrained with respect to the flux density (B), current (I) and each geometric parameter given by G. G is a set of critical geometrical parameters under consideration which are piston radius, piston core radius, pole length, gap thickness and cylinder thickness.

The optimization process yields a combination of a set of values for the critical parameters as shown in tables 4.1 and 4.2. The iterations are performed simultaneously on each variable, starting with the lower bound on variables, and the process stopped when the desired damping force in inactive and active states is achieved.

Optimized geometrical parameters are verified for the damping force requirements at no excitation and full excitation boundary conditions. Also the few iterations at equal interval are captured and show in the tabulated form below in Table 4.1 and Table 4.2.

The optimized MR damper geometry is then validated against the minimum and maximum damping force requirement. Figure 4.4 shows that the optimized damper geometry is capable of generating the damping force for the operational range of 726N-2150 N. The minimum and maximum damping force generated by optimized MR damper geometry is 821.9 N and 2183.6 N respectively.

Table 4.3 shows the optimized parameter values for piston radius, piston core radius, pole length, gap thickness, and cylinder thickness.

Table 4.1.
Optimization results at no excitation (I=0Amp) condition

Piston Radius (m)	**Piston Internal Radius (m)**	**Pole Length (m)**	**Gap Thickness (m)**	**Cylinder Thickness (m)**	**Damping force (N)**
0.015	0.006	0.012	0.001	0.007	278.4769
0.0162	0.0066	0.0125	0.00106	0.0076	386.2712
0.0174	0.0072	0.013	0.00112	0.0082	492.2786
0.0186	0.0078	0.0135	0.00118	0.0088	594.0756
0.0198	0.0084	0.014	0.00124	0.0094	690.5025
0.021	0.009	0.0145	0.0013	0.01	829.1039

Table 4.2.
Optimization results at full excitation (I=2Amp) condition

Piston Radius (m)	**Piston Internal Radius (m)**	**Pole Length (m)**	**Gap Thickness (m)**	**Cylinder Thickness (m)**	**Damping force (N)**
0.015	0.006	0.012	0.001	0.007	879.4
0.0162	0.0066	0.0125	0.00106	0.0076	1138.6
0.0174	0.0072	0.013	0.00112	0.0082	1374.8
0.0186	0.0078	0.0135	0.00118	0.0088	1585.1
0.0198	0.0084	0.014	0.00124	0.0094	1769.3
0.021	0.009	0.0145	0.0013	0.01	2187.4

4.5 Closure on the Chapter

Chapter 4 summarizes the MR damper geometry. The cross sectional view helps understanding the geometrical parameters, which affect the damping force generated

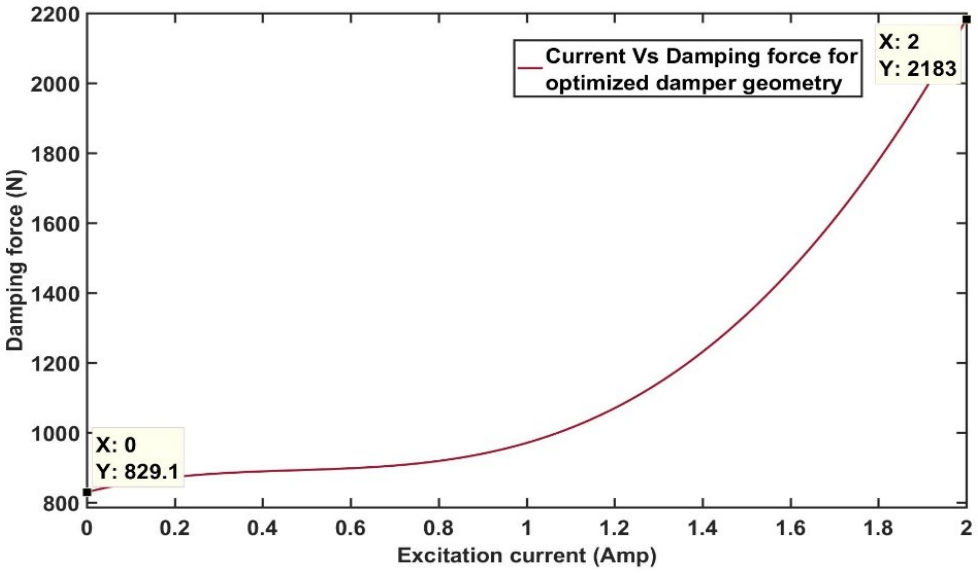

Fig. 4.4. Excitation current Vs Damping force characteristics for the optimized damper geometry

Table 4.3.
Optimized values of critical MR damper geometrical parameters

Critical geometrical parameters	**Optimized values (mm)**
Piston Radius (R)	21
Pole Length (L)	14.5
Gap thickness (g)	1.3
Cylinder Thickness (t)	10
Piston Internal Radius (Rc)	9

by the damper. Critical geometric parameters are determined for the MR damper design and geometric optimization. Sensitivity analysis is performed to analyze the unit change effect of considered parameters on the damping force generation. Gap thickness is observed as most sensitive parameter for the damper design and optimization. Also, multi objective MR damper geometric optimization is achieved for the desired range of operation. Optimization of MR damper shall be followed with

the robust control system implementation to further enhance the ride quality and vehicle handling performance. Chapter 5 focuses on PID control implementation of optimized MR damper active suspension with Bouc-Wen theory of hysteresis.

5. SYSTEM IDENTIFICATION AND PID CONTROLLER IMPLEMENTATION

5.1 PID Control Architecture and Significance of Controller Gains

PID controller is differentiated based on the architecture framework of the gains. The two main controller architecture are serial PID controller and parallel PID controller. In serial PID controller the proportional term obtained after error is processed through proportional gain is fed through integral and derivative gain, thus increases the overshoot as compared to the parallel PID controller [29]. One of the important goal of this research is minimize the overshoot due to the road disturbances with a minimum settling time. Parallel PID controller is implemented for the stated reason. Parallel PID controller is represented using the equation (5.1).

$$u(t) = K_p e(t) + K_i \int_0^t e(t)dt + K_d \frac{de(t)}{dt} \tag{5.1}$$

Significance of the each controller gain and its effect on the manipulated variables and process control is explained in the following subsections of the chapter.

5.1.1 Proportional Gain

Proportional gain depends on the difference between the set point (desired operating point) and the process variable state (value) at that moment. The difference between the set point and instantaneous process variable value is treated as error. Higher the proportional gain faster is the control system response, but increasing proportional gain causes the oscillations of process variable [29].

5.1.2 Integral Gain

Integral gain is often termed as steady state error eliminator. Integral gain accumulate the error over time. Unless zero error state is achieved, a small error term causes integral component to increase over a time. Integral windup occurs when integral action saturates the controller [29].

5.1.3 Derivative Gain

Derivative component of PID reacts to the rate of change of error term. If the system variables have higher rate of change derivative gain causes system output to decrease. Derivative time parameter increase causes the controller to act more strongly and rapidly against the error term. Usually derivative gain is kept very small as it is sensitive to the noisy signal [29].

5.2 System Identification

The suspension system is modeled as a non-linear system, and thus linearized at each operating point with an approximation [30, 31]. The linear system is then identified to determine the transfer function. The road input is considered as open loop input and the sprung-mass displacement is considered as the open loop output for the linearization and system identification. System identification facilitated the conversion of suspension plant model into state space model and transfer function. The transfer function allows to analyze the stability of the system during additional pole consideration for the PID controller design. State space of the Bouc-Wen MR suspension model is explained in the following subsections.

5.2.1 State Space Model of System

The identification of the linearized system yields the following state-space model, which is an equivalent representation of the Bouc-Wen Model. The determined state-space model is as follows:

$$A = \begin{bmatrix} 0 & 1 & 0 & 0 & 0 \\ -32.12 & -1.9 & 0.14 & 32 & -4.349 \\ 2.031 & 12.66 & -48.03 & -1813 & 33.98 \\ 0 & 0 & 1 & 0 & 0 \\ 0 & 1.5 & 0 & 0 & 0 \end{bmatrix} \tag{5.2}$$

$$B = \begin{bmatrix} 0 \\ 0 \\ 1563 \\ 0 \\ 0 \end{bmatrix} \tag{5.3}$$

$$C = \begin{bmatrix} 1 & 0 & 0 & -1 & 0 \end{bmatrix} \tag{5.4}$$

$$D = \begin{bmatrix} 0 \end{bmatrix} \tag{5.5}$$

Where, A is the system matrix, defines the states of the suspension over the operational range, given by equation (5.2).

B is input matrix, defines the state of road disturbance experienced by the vehicle body given by equation (5.3).

C is the output matrix, shows the sprung mass displacement due to road disturbances given by equation (5.4).

D is the feedforward matrix, system input and output was defined as open loop signals, and thus it is a zero vector given by equation (5.5).

State space model is further processed to obtain the transfer function of the suspension system. Transfer function is then utilized for the PID controller implementa-

tion. Transfer function determination and PID controller implementation is explained in the subsequent subsections.

5.2.2 Transfer Function Determination

Transfer function is a representation of plant model, which is nothing but a ratio of sprung mass displacement to the road disturbance experienced by the vehicle body. Transfer function is determined from the state space model derived in the previous subsection. Equation (5.6) – (5.8) are used to derive the suspension system transfer function from obtained state space model vectors.

$$\dot{X} = AX + BU \tag{5.6}$$

$$Y = CX + DU \tag{5.7}$$

$$Y(s) = [C(sI - A)^{-1}B + D]U(s) \tag{5.8}$$

Substituting the state space vectors into equation (5.8), transfer function of the MR damper suspension system with Bouc-Wen hysteresis is derived as follows using equation (5.9) – (5.10):

$$Y(s) = \{ \begin{bmatrix} 1 & 0 & 0 & -1 & 0 \end{bmatrix} \Big(s \begin{bmatrix} 1 & 0 & 0 & 0 & 0 \\ 0 & 1 & 0 & 0 & 0 \\ 0 & 0 & 1 & 0 & 0 \\ 0 & 0 & 0 & 1 & 0 \\ 0 & 0 & 0 & 0 & 1 \end{bmatrix} -$$

$$\begin{bmatrix} 0 & 1 & 0 & 0 & 0 \\ -32.12 & -1.9 & 0.14 & 32 & -4.349 \\ 2.031 & 12.66 & -48.03 & -1813 & 33.98 \\ 0 & 0 & 1 & 0 & 0 \\ 0 & 1.5 & 0 & 0 & 0 \end{bmatrix} \Big)^{-1} \times \tag{5.9}$$

$$\begin{bmatrix} 0 \\ 0 \\ 1563 \\ 0 \\ 0 \end{bmatrix} + \begin{bmatrix} 0 \end{bmatrix} \} U(s)$$

$$G(s) = \frac{Y(s)}{U(s)} \tag{5.10}$$

Transfer function of the suspension plant model is given by equation (5.11).

$$G(s) = \frac{-1563s^3 - 2750s^2 - 1.038 \times 10^4 s - 5.192 \times 10^{-13}}{s^5 + 49.93s^4 + 1941s^3 + 4887s^2 + 6.835 \times 10^4 s - 1.566 \times 10^{-10}} \tag{5.11}$$

The determined transfer function response is then compared with the system model response. The comparison shows that responses are in 98.10 percent agreement for the rise time and 88 percent match for the slew rate as shown in figure 5.1. Transfer function and plant model response comparison is observed for the default impulse input using the system identification toolbox of MATLAB software package.

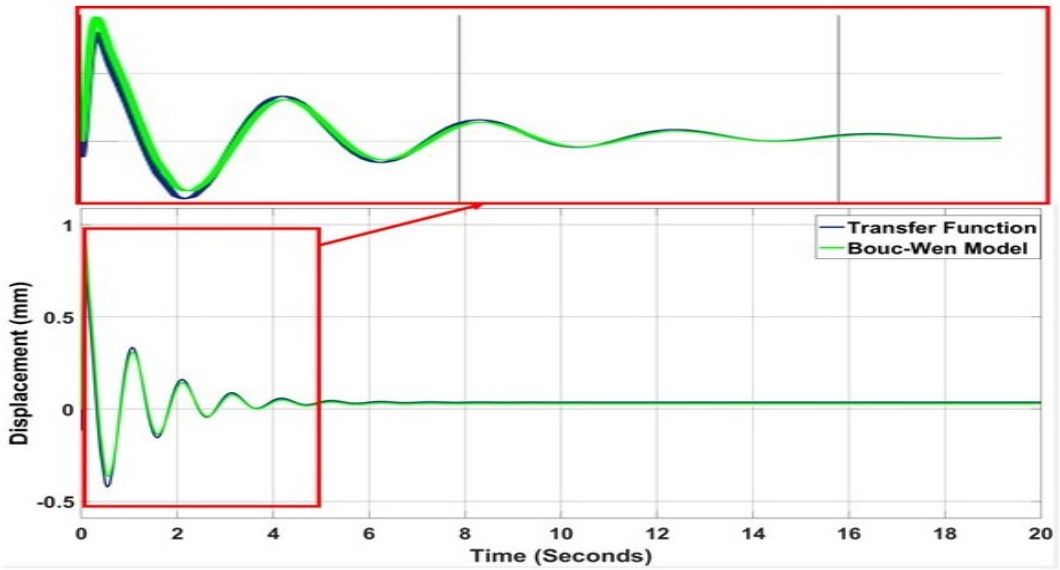

Fig. 5.1. Comparison of transfer function and system model response

5.3 PID Controller Implementation

PID controller is designed to reduce the error between the reference road input signal and sprung-mass displacement. The minimization of the error ensures the adherence of vehicle sprung-mass mounted on the suspension mount for a given road profiles. The reduced displacement and vibration offers required comfort to driver as well as passenger. Zeigler-Nicholas method is used to determine initial control gains. Parallel approach of the PID is used for the controller design as given by the equation (5.1). Taking into consideration of all the controller gain effects, PID controller is designed for the Bou-Wen MR suspension model. PID controller characteristic in Laplace form is given by equation (5.12).

$$G_c(s) = \frac{sK_p + K_i + s^2K_d}{s} \tag{5.12}$$

The overall closed loop transfer function, T(S) is given by the equation (5.13).

$$T(s) = \frac{G(s)G_c(s)}{1 + G(s)G_c(s)} \tag{5.13}$$

$$T(s) = \frac{\frac{-1563s^3-2750s^2-1.038\times10^4 s-5.192\times10^{-13}}{s^5+49.93s^4+1941s^3+4887s^2+6.835\times10^4 s-1.566\times10^{-10}} * \frac{sK_p+K_i+s^2K_d}{s}}{1+\frac{-1563s^3-2750s^2-1.038\times10^4 s-5.192\times10^{-13}}{s^5+49.93s^4+1941s^3+4887s^2+6.835\times10^4 s-1.566\times10^{-10}} * \frac{sK_p+K_i+s^2K_d}{s}} \tag{5.14}$$

The denominator of the characteristic equation (5.14) is then compared with the denominator of the equation (5.13). The denominator of the T(s) is determined as follows:

$$\begin{aligned} Den = \\ s^6 + (49.93 - 1563K_d)s^5 + \\ (1941 - 1563K_p - 2750K_d)s^4 + \\ (4887 - 2750K_p - 1563K_i - 10380K_d)s^3 + \\ (6.835\times10^4 - 10380K_p - 2750K_i - 5.192\times10^{-13})s^2 + \\ (-1.566\times10^{-10} - 5.192\times10^{-13}K_p - 10380K_i)s + 5.192\times10^{-13}K_i \end{aligned} \tag{5.15}$$

The characteristic equation comparison shows that the 4 additional poles required to be considered. Root locus analysis is shown in the figure 5.2, shows that the considered additional poles shall be less than the -24 on the real axis for the stability of the system designed. The additional poles considered are -30, -40, and -50 on the real axis.

Controller gains obtained are then modeled into the closed loop Bouc-wen suspension plant model for the closed loop (controlled) response simulation. Chapter 6 focuses on closed loop (controlled) simulation of Bouc-Wen MR suspension model. Modeled system is tested for six road profiles described in section 3.1.

5.4 Closure on the Chapter

Chapter 5 summarizes the uniqueness of the developed suspension system when compared to the previous research conducted in the area of active suspension. PID control architecture is summarized in the section 4.1. Section 4.2 documents the system identification techniques for the Bouc-Wen MR suspension model. System state space model and transfer function is well explained though the same. PID

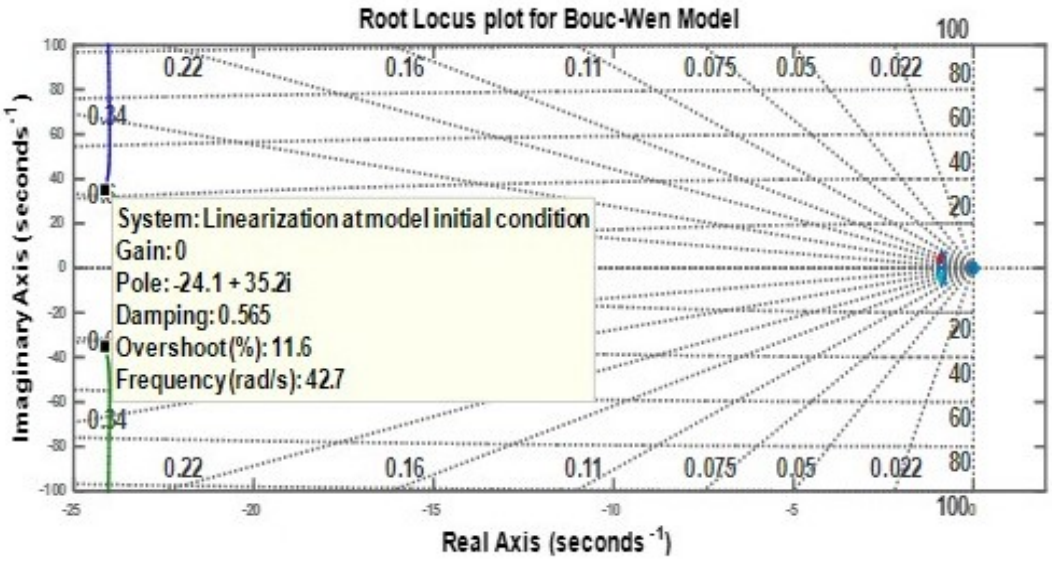

Fig. 5.2. Root-locus plot of Bouc-Wen MR suspension model

controller design and implementation considering stability of the system is explained in the section 5.3. Chapter 6 focuses on controlled responses obtained by simulation of the modeled system.

6. CONTROLLED SIMULATION OF SUSPENSION PLANT MODEL WITH PID CONTROLLER

PID controller is implemented with an aim of reducing the sprung mass displacement due to road disturbance without compromising on the settling time. This chapter compares the controlled and uncontrolled responses of the Bouc-Wen model for five different road profiles. The proportional, integral, and derivative gains designed for the PID controller minimizes the error signal between the reference signal and open loop output which results into better performance. The controller provides a better damping control as compared to the open loop model. The performance improvement has been subsequently validated in the following figures.

The uncontrolled and controlled active suspension with MR damper are compared considering the Bouec-Wen model with hysteresis. Figure 6.1 and 6.2 shows the comparative response for the step road input, which simulates the sudden bump of 75 mm in the road. The controlled suspension shows the 55.27 percent decrease in overshoot compared to the uncontrolled system. Figure 6.3 and 6.4 shows the 81.96 percent overshoot reduction when the sinusoidal road profile with the amplitude of 75 mm and frequency of 20.8 rad/sec are used. Figure 6.5 and 6.6 simulates the white noise input for the developed suspension model. 56.47 percent improvement in overshoot has been observed after the PID controller implementation. Figures 6.7 and 6.8 show 61.60 percent overshoot improvement for the random and uncertain road profile. Mixed road input is used to simulate the uncertain and wavy road profile and the controlled response shows 61.50 percent improvement in overshoot as shown in figures 6.9 and 6.10. The road type C is used for the real time road profile simulation and there is 17.89 percent overshoot improvement using PID controller as shown in figures 6.11 and 6.12. The overshoot improvement for each road profile is achieved without compromising on the settling time response.

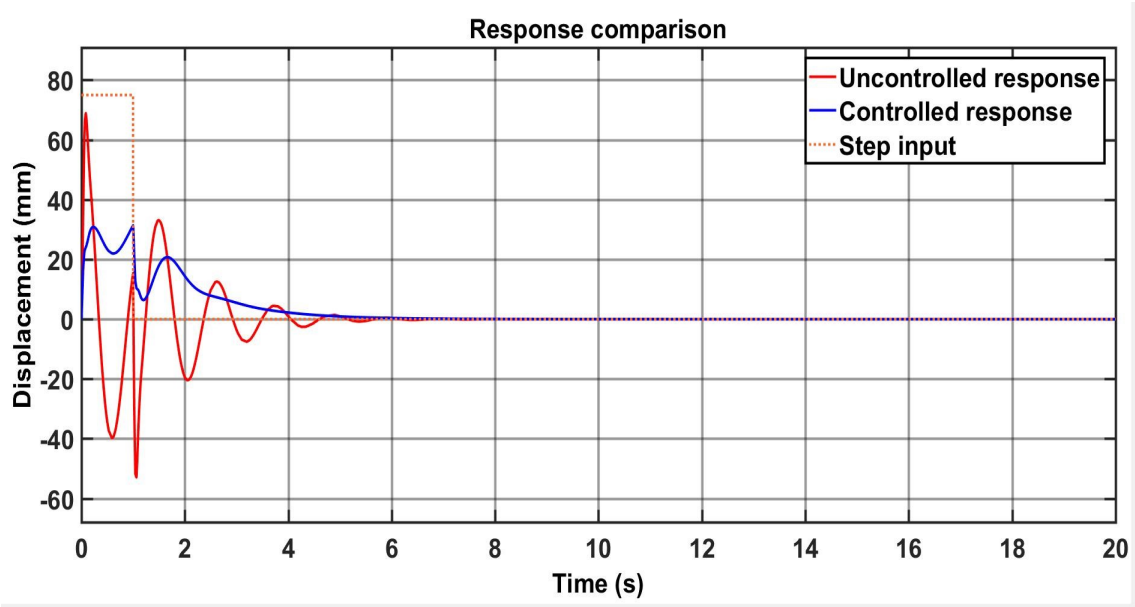

Fig. 6.1. Comparative response for controlled and uncontrolled Bouc-Wen model for step road input

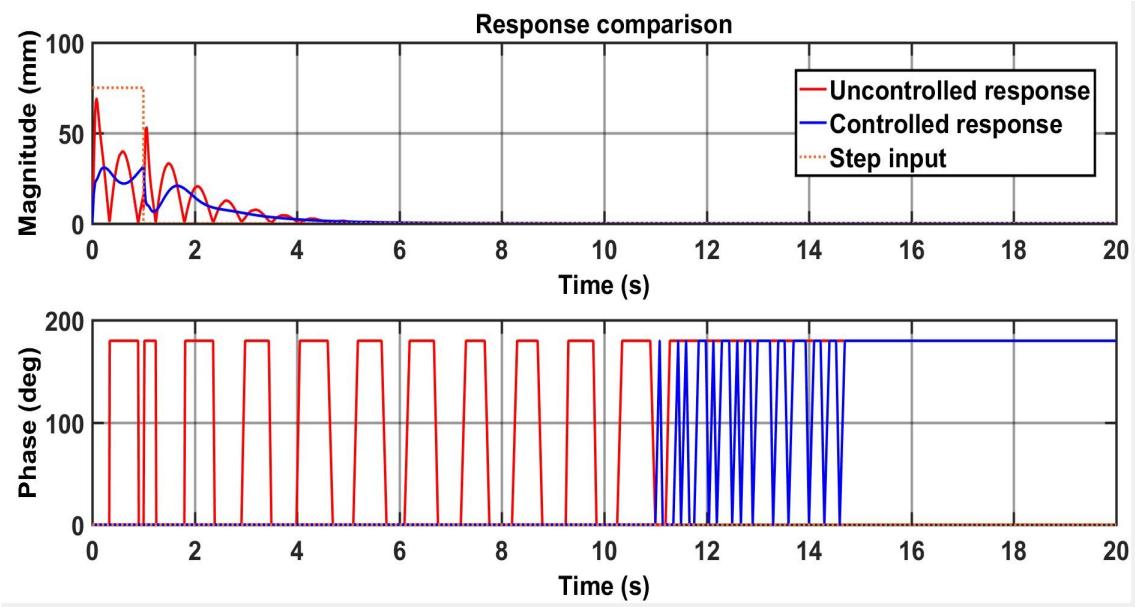

Fig. 6.2. Comparative magnitude and phase response for controlled and uncontrolled Bouc-Wen model for step road input

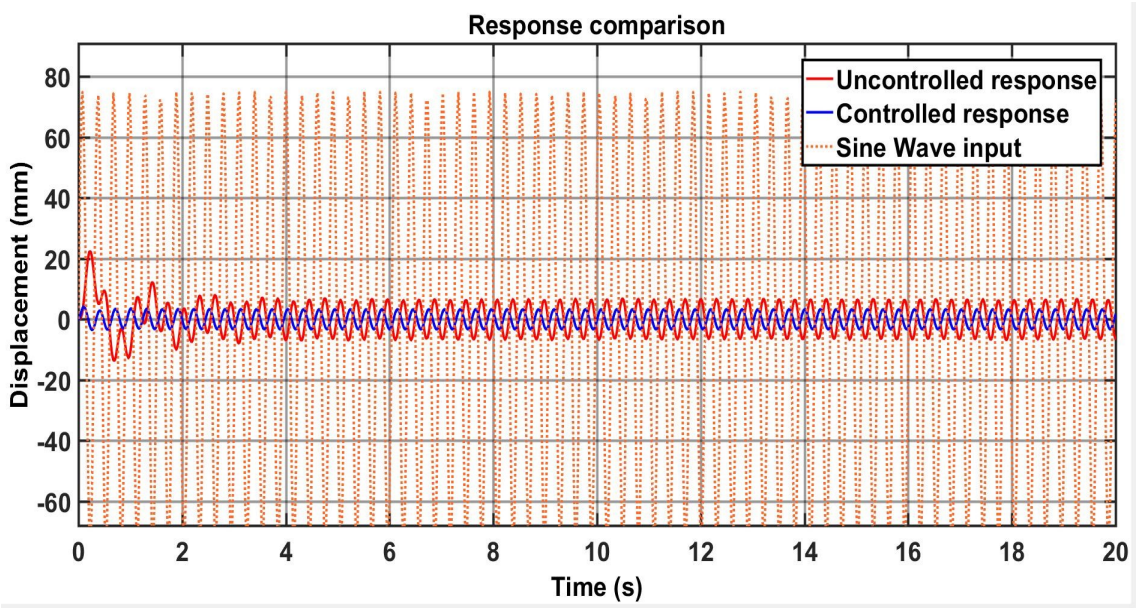

Fig. 6.3. Comparative response for controlled and uncontrolled Bouc-Wen model for sine road input

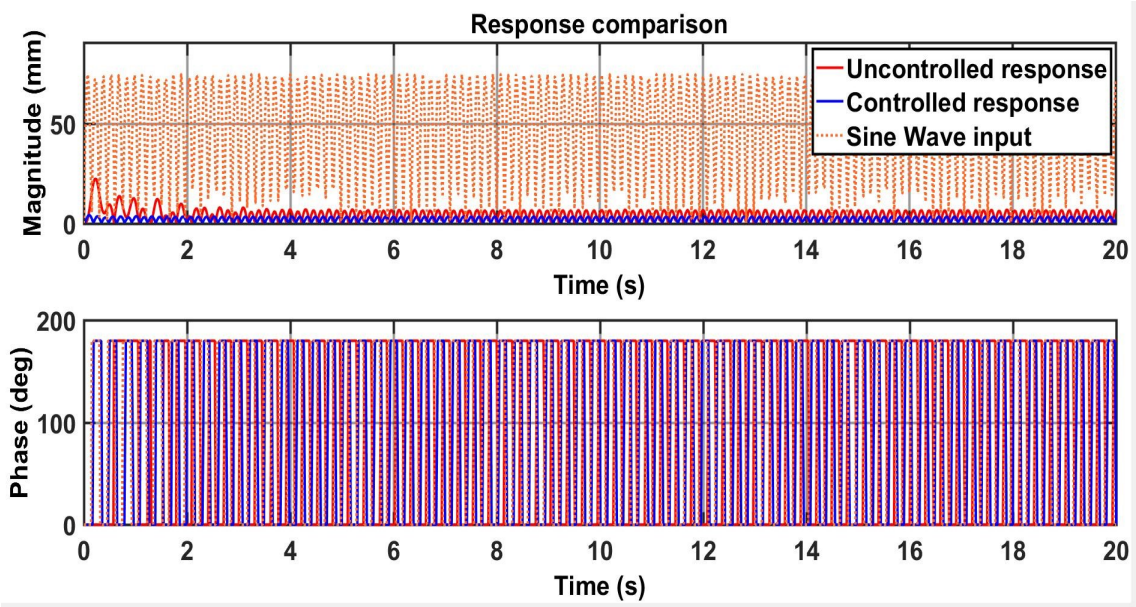

Fig. 6.4. Comparative magnitude and phase response for controlled and uncontrolled Bouc-Wen model for sine road input

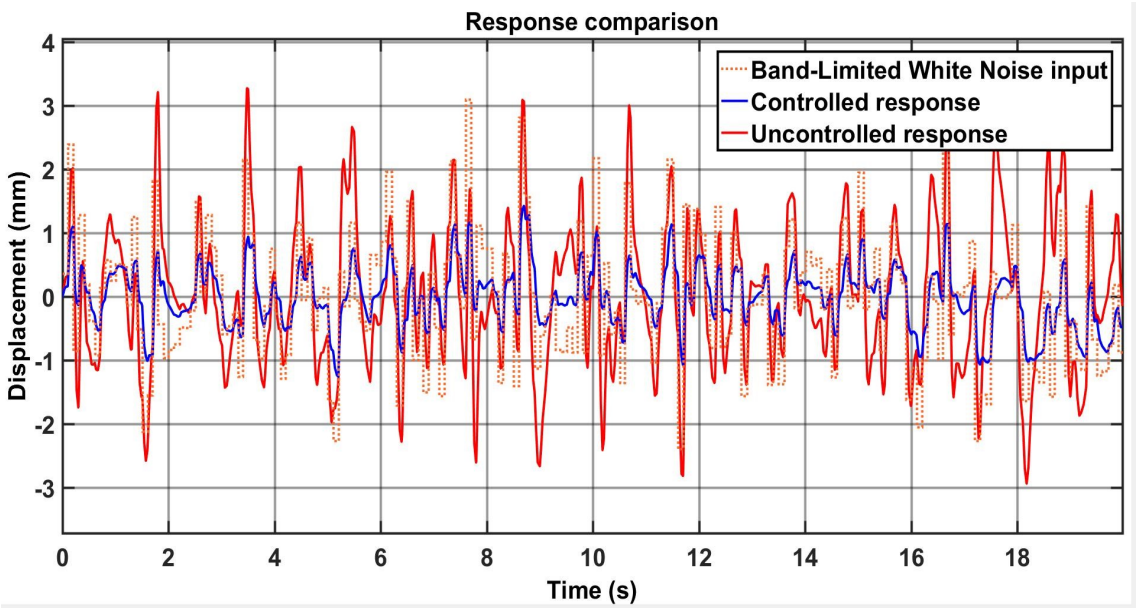

Fig. 6.5. Comparative response for controlled and uncontrolled Bouc-Wen model for white noise road input

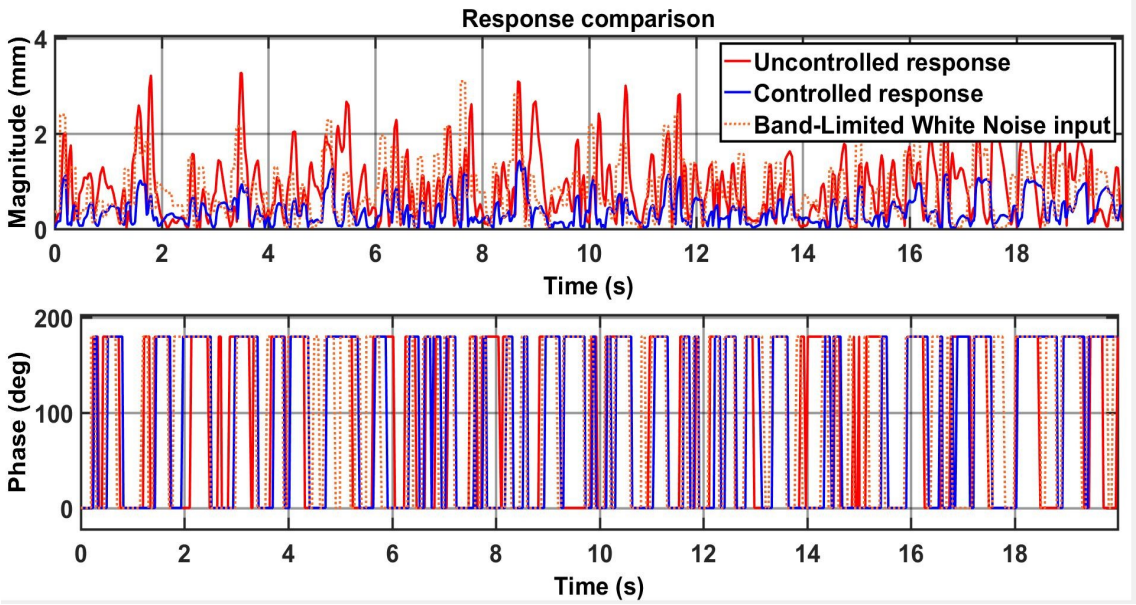

Fig. 6.6. Comparative magnitude and phase response for controlled and uncontrolled Bouc-Wen model for white noise road input

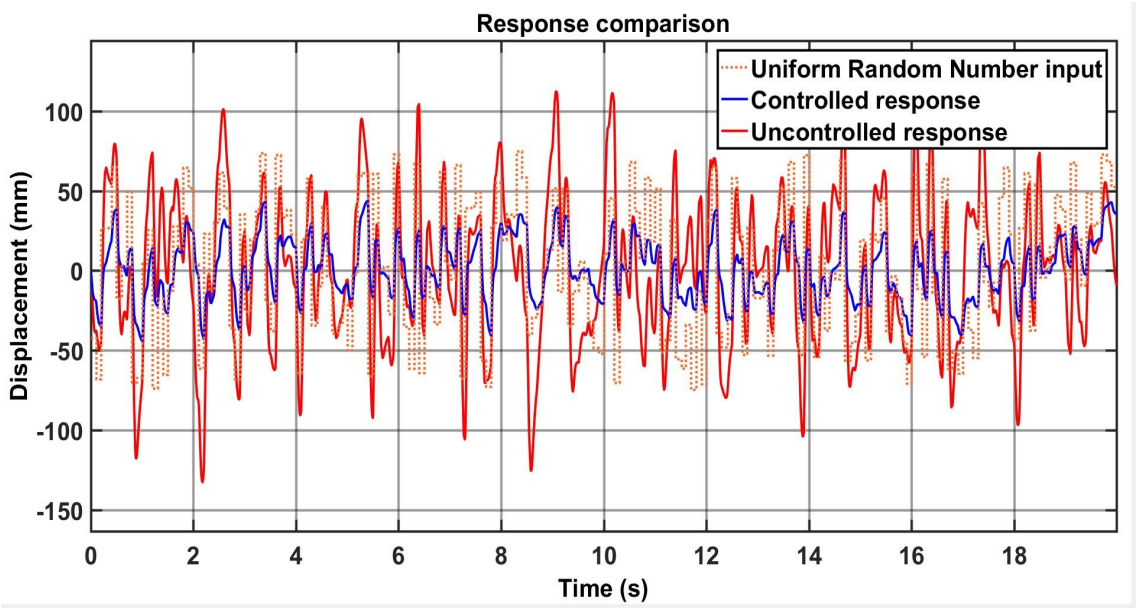

Fig. 6.7. Comparative response for controlled and uncontrolled Bouc-Wen model for uniform random number road input

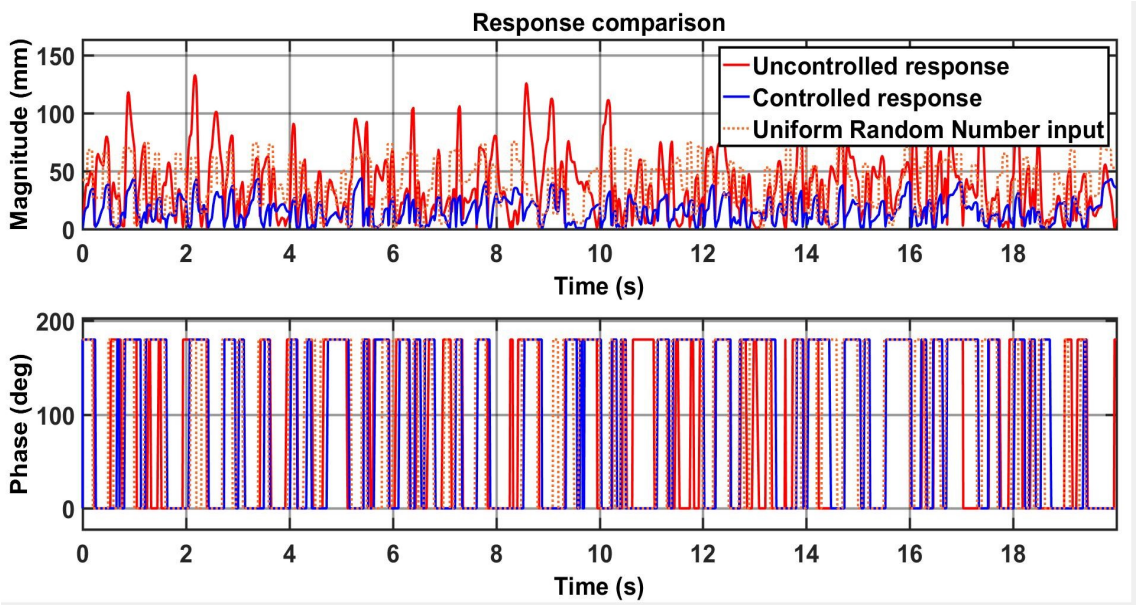

Fig. 6.8. Comparative magnitude and phase response for controlled and uncontrolled Bouc-Wen model for uniform random number road input

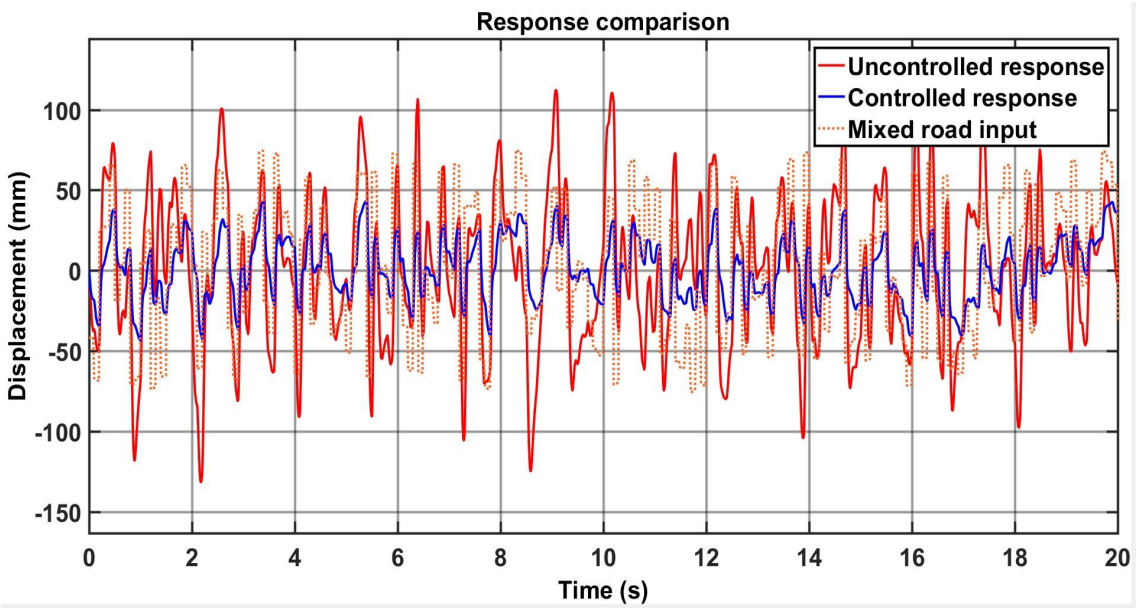

Fig. 6.9. Comparative response for controlled and uncontrolled Bouc-Wen model for mixed road input

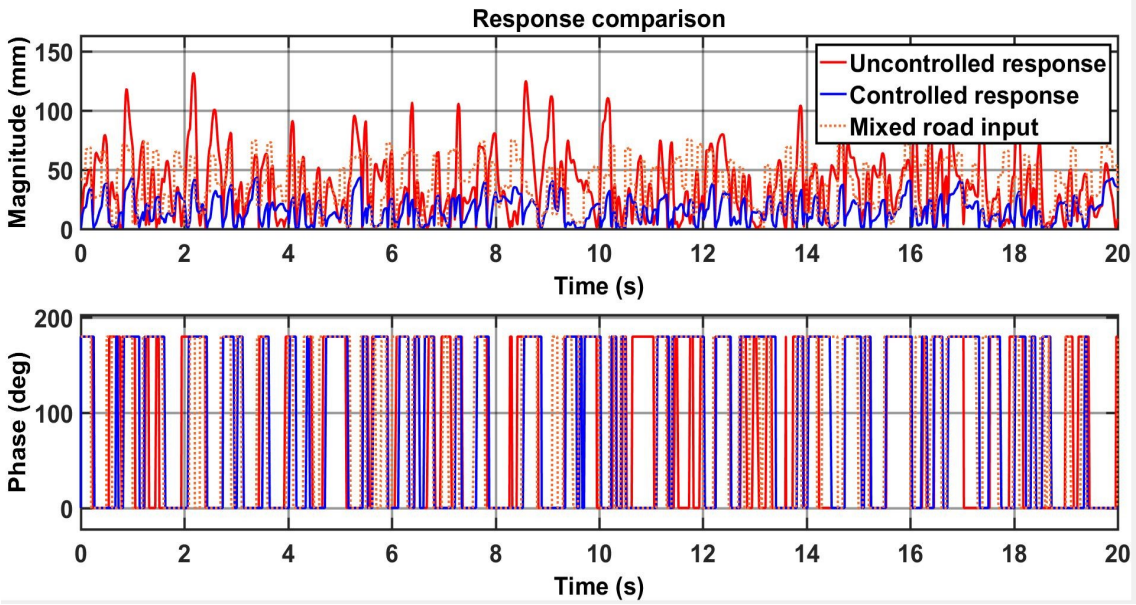

Fig. 6.10. Comparative magnitude and phase response for controlled and uncontrolled Bouc-Wen model for mixed road input

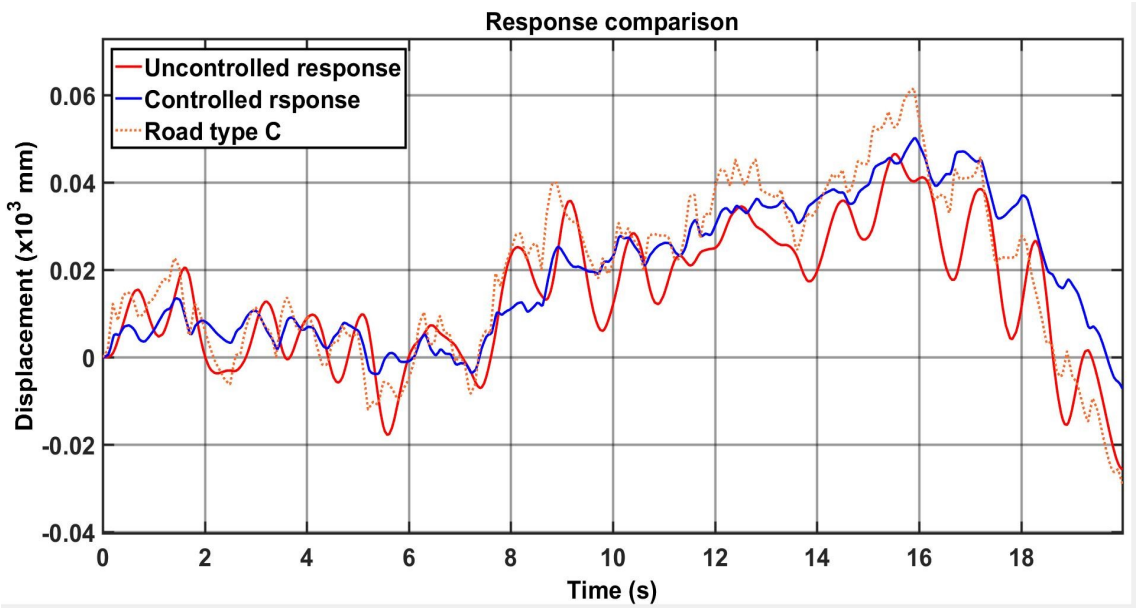

Fig. 6.11. Comparative response for controlled and uncontrolled Bouc-Wen model for road type C input

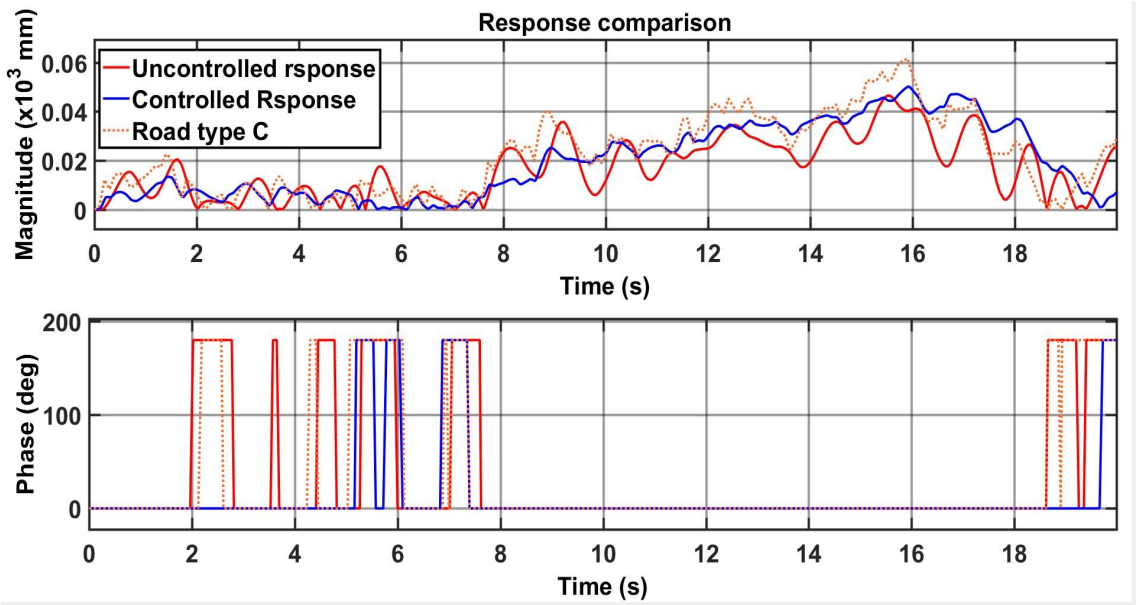

Fig. 6.12. Comparative magnitude and phase response for controlled and uncontrolled Bouc-Wen model for road type C input

6.1 Closure on the Chapter

Controlled responses for the modeled plant simulation is acknowledged in this chapter. The comparison of controlled and uncontrolled responses of Bouc-Wen MR suspension model for all six road inputs are analyzed. The percentage improvement in the overshoot is calculated with PID controller implementation, and it has been observed that the designed PID controller holds good for all the tested road disturbance profiles. This chapter summarizes the mathematical modeling, simulation, and analysis of the MR suspension model with Bouc-Wen hysteresis. Systems engineering approach is taken for the system level, subsystem level, and component level design of the active suspension MR damper. The systems engineering is explained in chapter 7.

7. SYSTEMS ENGINEERING APPROACH AND MBSE MODEL DEVELOPMENT FOR ACTIVE SUSPENSION MR DAMPER

7.1 Systems Engineering Overview

MR dampers have been a great introduction in the field of automotive suspension. MR damper has been proven to be a highly effective yet complex system. Systems engineering provides an approach to provide solution to technologically challenging and complex problems [32–34]. System architecture development, probable failure mode analysis, interface architecture definition for robust system, risk management, increased productivity, and superior quality are some of the inherent advantages of applying systems engineering principles to product development cycle. The importance of systems engineering principle application is well explained through cost of change tradeoff with respect to phase of product development cycle as shown in the figure 7.1.

Model based systems engineering (MBSE) approach has been taken for this research and systems engineering principles are applied towards the active suspension MR damper design and development. MBSE is model based definition of specification, requirements and design, which surpasses the document based systems engineering approach. Also, with the help of computer aided tool MBSE facilitates the design of system as whole. Major advantages of systems engineering are listed below [36–42].

- Access of all information under single framework
- Channeled information flow at every stage of product development
- Continuous progress tracking with modeling languages and graphical representation of system

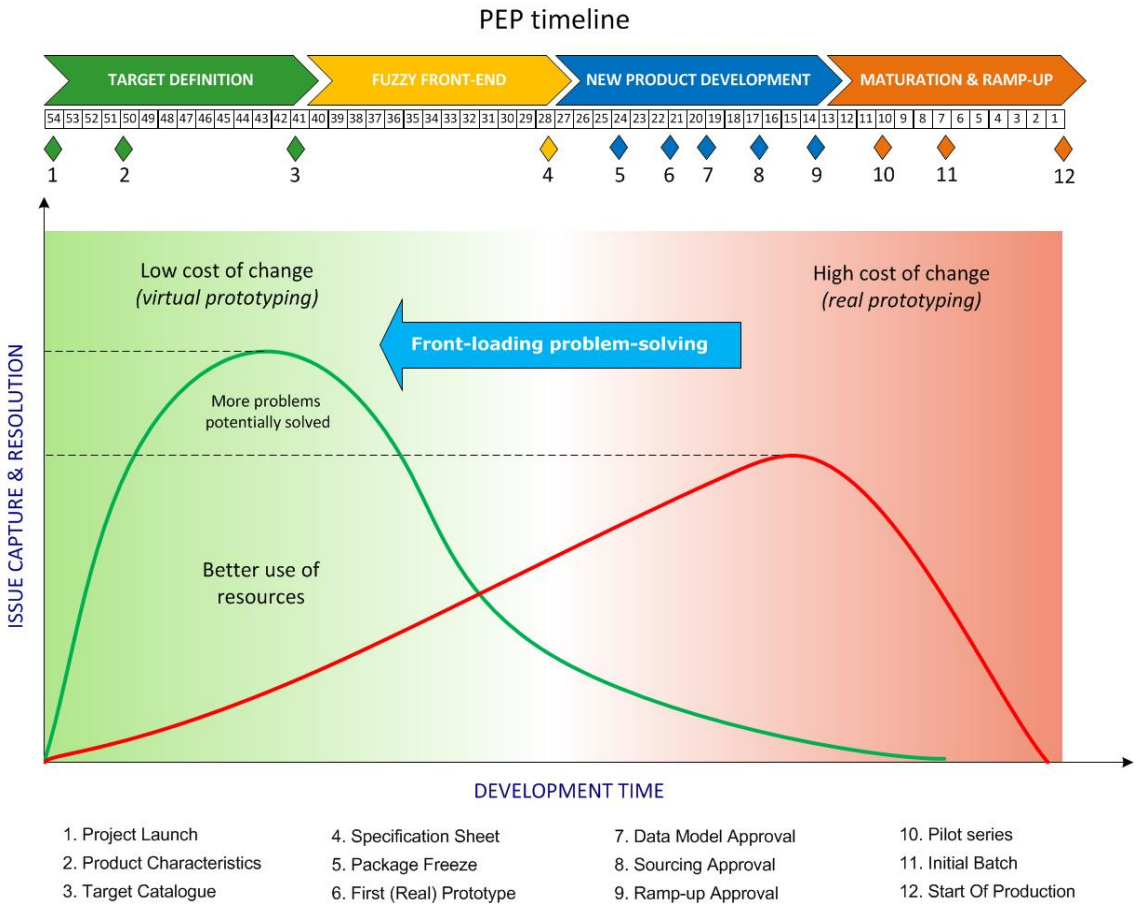

Fig. 7.1. Product development phase Vs cost of change trade off [35]

- Continuous change effect analysis during and after development of product
- Enhanced communication
- Leveraging models through a product development lifecycle
- Enhance knowledge transfer
- Requirement traceability

Above stated advantages encourages the MBSE approach for the MR damper requirements analysis, development, and validation. FAST diagram for MR damper facilitates the decomposition of requirements from the stakeholder (passenger comfort

and vehicle handling performance) to system component level [43, 44]. Value streaming map/value flow map focuses on the information flow between the subsystems of MR damper such as electromagnet, MR fluid, damper geometry, vehicle body, and road disturbances. Boundary diagram explains the major interfaces of MR damper system and subsystem. Boundary diagram is an essential input for determination of failure modes. Figure 7.2 shows the milestones in MBSE model development for MR damper. MagicDraw system modeler is used for the MBSE model development of MR damper after the application of systems engineering principles explained in this section.

MBSE approach taken is subcategorized into three main steps stated below:

- MR damper requirement analysis for Bouc-Wen active suspension system
- MR damper design and modeling based on the system requirements
- Parametric analysis and requirement traceability of the developed model

Parametric analysis and requirement traceability is carried out by integrating the MR damper developed using MATLAB and MBSE model developed using MagicDraw system modeler [45–47].

7.2 Systems Engineering Tool Application for Active Suspension MR Damper

Identifying the requirements of MR damper is the primary goal of FAST diagram [43, 44]. Requirements identification is followed by generating the system context. Boundary diagram is used for defining the system boundaries and major interface and communication between the subsystems of MR damper. System context helps in failure mode effect analysis based on the requirements determined using FAST diagram and interfaces defined by boundary diagram. This also helps understanding the critical parameter analysis. Sensitivity analysis of geometrical parameters defined in the section 4.2 results a supplementary action. Value streaming map is generated

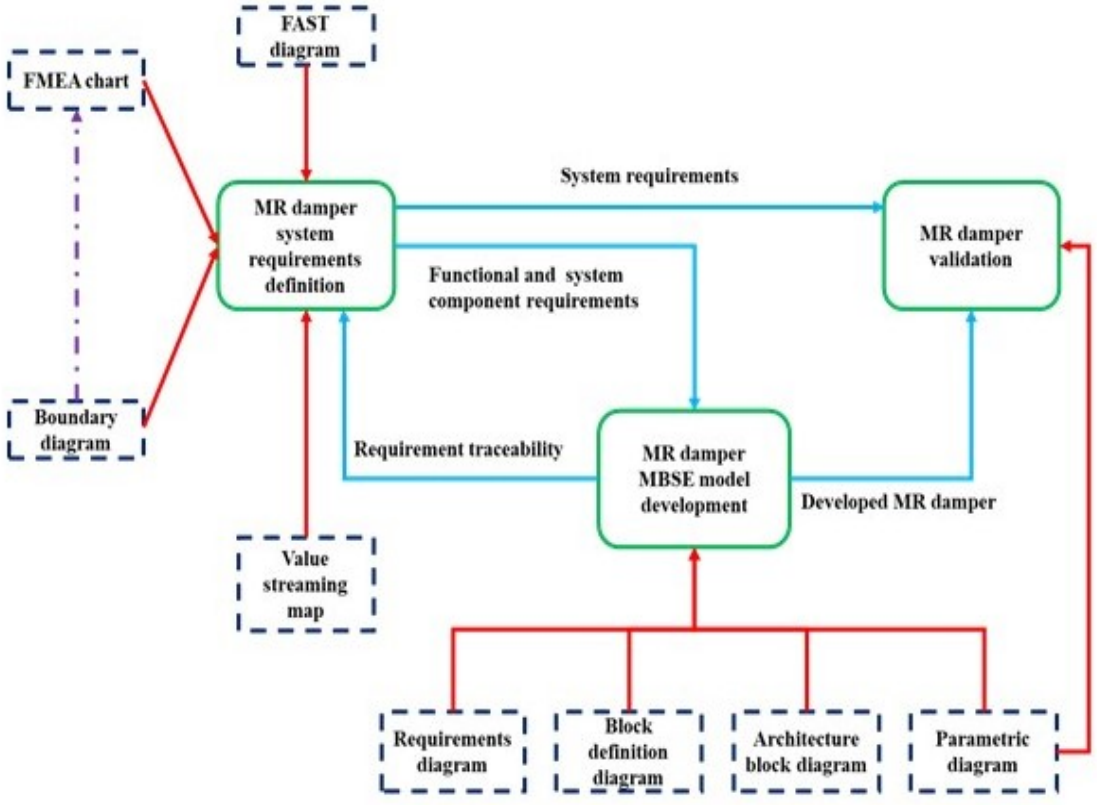

Fig. 7.2. MBSE approach milestones in MR damper development

once the major interfaces of the system is determined, which explains the information flow between components and subsystems. All the above mentioned systems engineering tools are explained in the subsequent subsections.

7.2.1 FAST Diagram

FAST is an abbreviation of functional analysis system techniques. FAST diagram facilitates the functional decomposition of requirements from the high level system to component level functional requirements. Cross-functional approach is taken to define the functional requirement decomposition of MR damper into component level requirements. Functional level requirements are first decomposed into the subsystem

level requirements, which also helps in understanding the dependencies of subsystem for the operational behavior. Figure 7.3 shows the FAST decomposition of active suspension MR damper from system to subsystem level functional requirements. This also helped in defining the subsystem and decomposing it to component level requirements. Major subsystems of MR damper are listed below.

- Damper geometry
- MR fluid
- Electromagnet
- Piston displacement and velocity module

Figure 7.4 shows the subsystem to component level decomposition of requirement to meet the design and functional objectives.

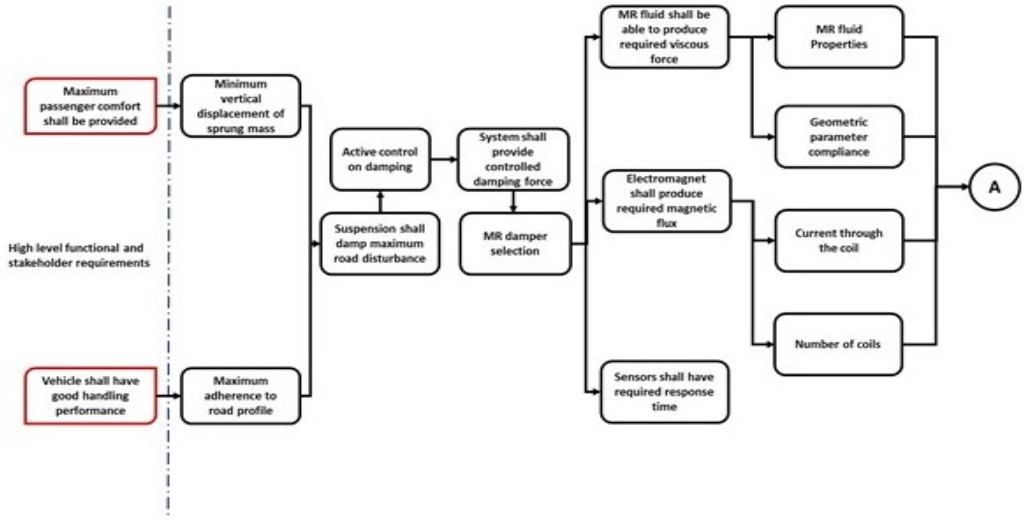

Fig. 7.3. MR damper system level functional requirement decomposition into subsystem level requirements using FAST technique

FAST diagram if read from left to right gives an answer how to achieve the desired functional requirements, and right to left flow show why the selection of particular

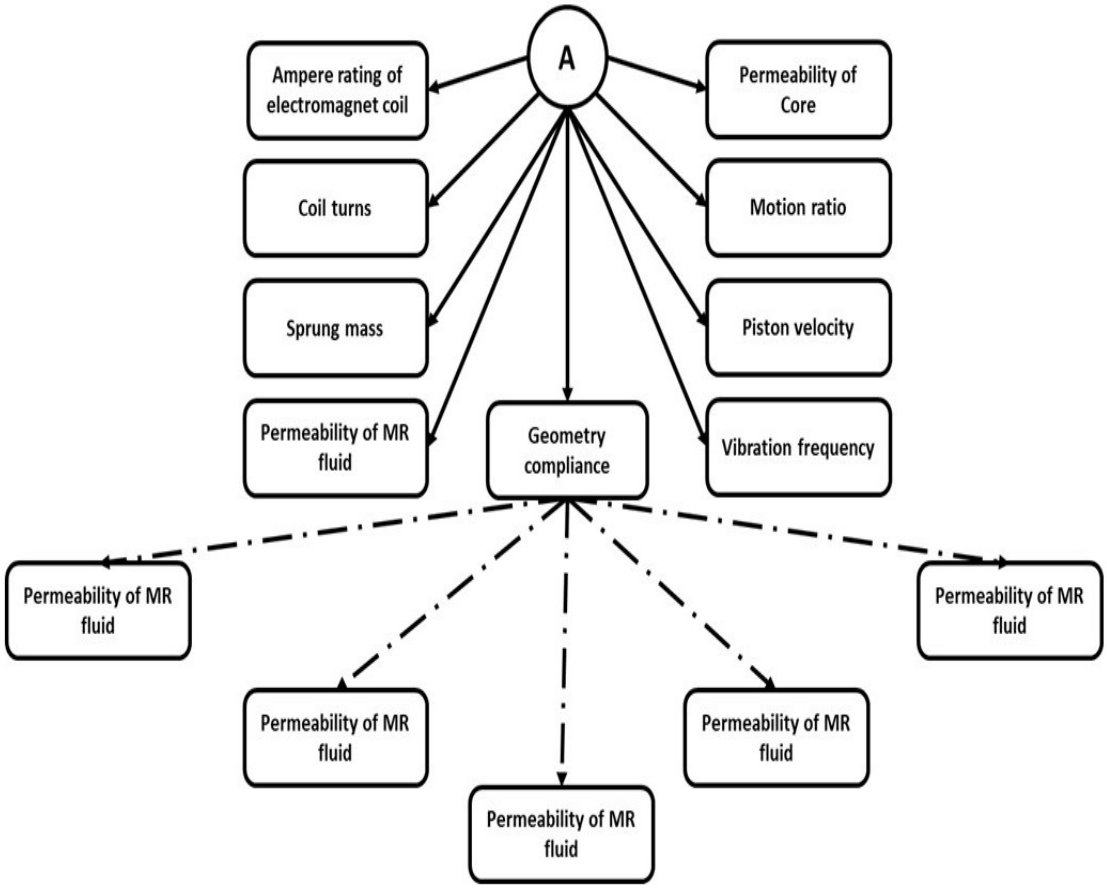

Fig. 7.4. MR damper subsystem level functional requirement decomposition into component level requirements using FAST technique

component is important to achieve system level goals. The MBSE requirements diagram modeled using MagicDraw is explained in section 7.3.1.

7.2.2 Boundary Diagram

Boundary diagram is used to define the scope of the system design. Also, boundary diagram simplifies process of understanding what requirements each system, subsystem, and component shall satisfy to meet the system level goals [48]. Interaction of each subsystem with the system defines the system of system. External interaction are also documented in boundary diagram. Boundary diagram helps in understanding

the potential failure modes, as previous research in the field shows that the maximum system failures occur at the interfaces.

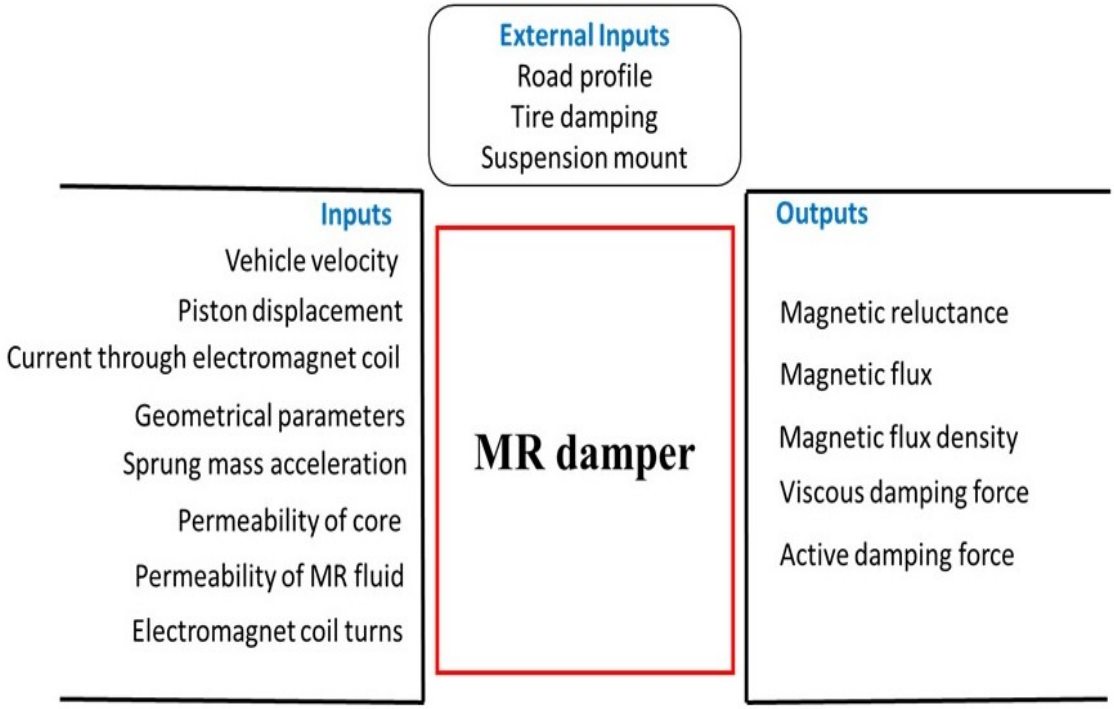

Fig. 7.5. MR damper boundary diagram

Developed boundary diagram for MR damper shown in figure 7.5 facilitates to understand the system input, system outputs, and external interaction of the system to perform desire operations. Major system inputs, outputs, and external interactions are listed below.

System inputs:

1. Vehicle velocity
2. Piston displacement
3. Electromagnetic coil current
4. Geometrical parameters

5. Sprung mass acceleration
6. Permeability of core.
7. Permeability of MR fluid.
8. Electromagnet coil turns

System outputs:

1. Magnetic reluctance
2. Magnetic flux
3. Magnetic flux density
4. Viscous damping force (In both inactive and active state)
5. Active damping force

External inputs/ interactions:

1. Road profile (Road roughness)
2. Tire damping (Assisting inactive and active damping of MR damper)
3. Suspension mount (Critical parameter which affect the damping force requirement)

Boundary diagram for MR damper helps in modeling the block definition diagram (BDD) and internal block (IBD) diagram using MBSE approach. Interfaces defined in this diagram can also be observed in the internal block diagram. BDD and IBD are well explained in section 7.3.2 and section 7.3.3 respectively.

7.2.3 Value Streaming Map

Value streaming map is a special flow chart which helps in understanding the overall data flow through and between system, subsystem, and components of the system. I/O interfaces between the system and environment, each subsystem, and between the components of same and other subsystem is defined using value streaming map [49–51]. Value streaming map drawn for the MR damper design is shown in figure 7.6.

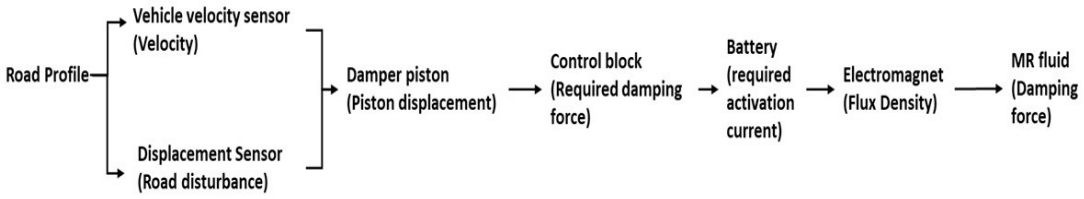

Fig. 7.6. MR damper value streaming map

Parametric (par) diagram is created based on the inputs of value streaming map. Interactions and data flow between the system, environment, subsystem, and components of MR damper is well captured in the value streaming map. Boundary diagram provides the initial inputs for defining the value streaming map of MR damper. Parametric diagram created based on the value streaming map using MagicDraw system modeler is explained in section 7.3.4.

7.3 MagicDraw Nomagic Cameo Model for MBSE Approach

FAST diagram, boundary diagram, and value streaming map of MR damper explained in the sections above enables MBSE model development of MR damper. Requirements diagram (Req), Block definition diagram (BDD), internal block diagram (IBD), and parametric diagram (Par) are explained in the subsequent sections. Parametric diagram is integrated with the MATLAB software package for the para-

metric simulation of developed MBSE model and requirement traceability. Validation approach and the process flow for the MR damper design is explained in the Figure 7.7.

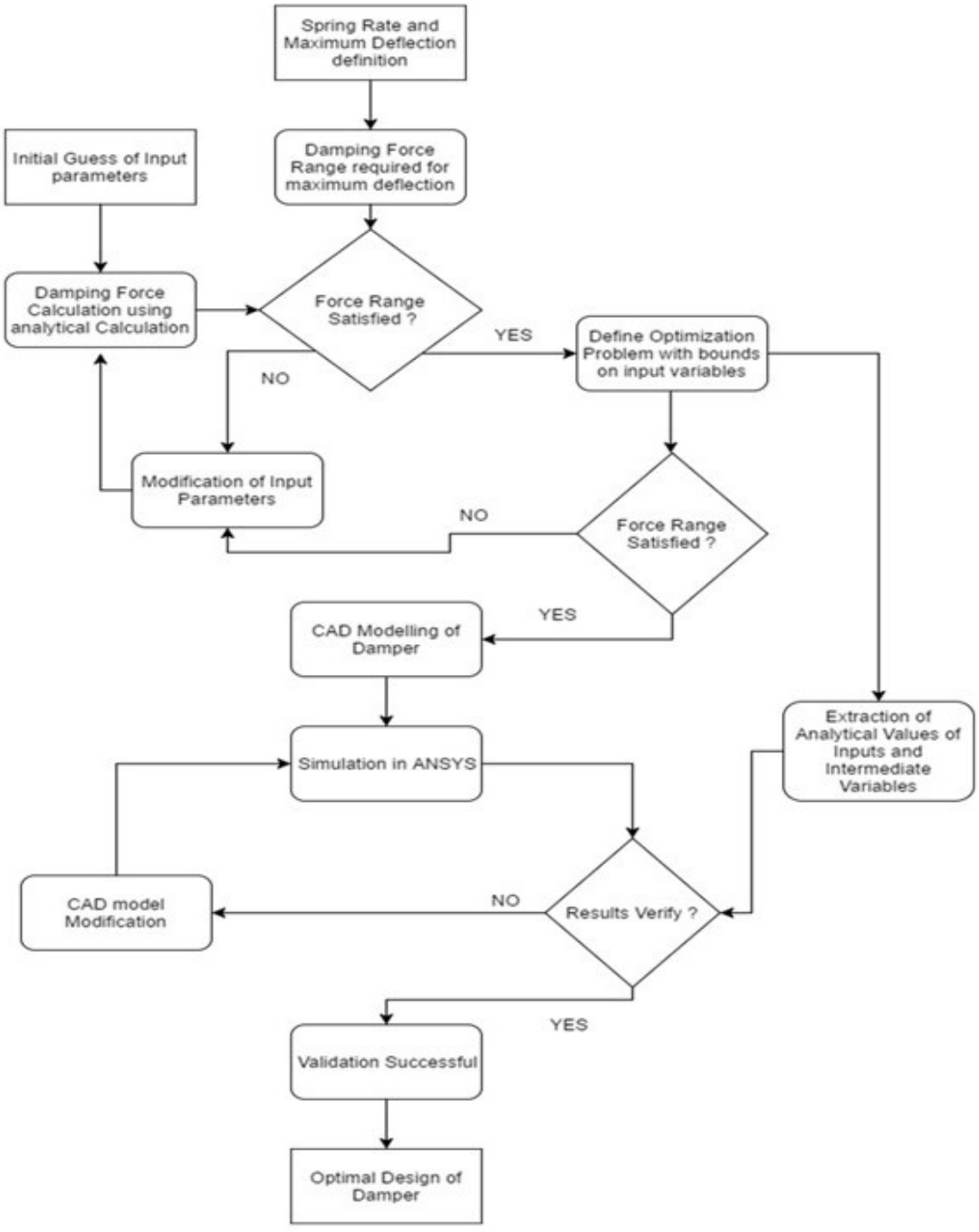

Fig. 7.7. Process flow and validation approach for MR damper design

7.3.1 Requirements Diagram

Requirements specifies the capability or condition that must be satisfied. Requirements are often used to define the objective of the system that is being modeled. Requirements elaborates the function that performed by the system. The decomposition of the system also facilitates to define system level requirements, subsystem level requirements, and component level requirements for system, subsystem, and each component of the system respectively. Following are the requirements for the Magnetorheological damper design and optimization obtained from the FAST technique. Figure 7.8 shows the requirements diagram developed for MR damper design using MagicDraw system modeler.

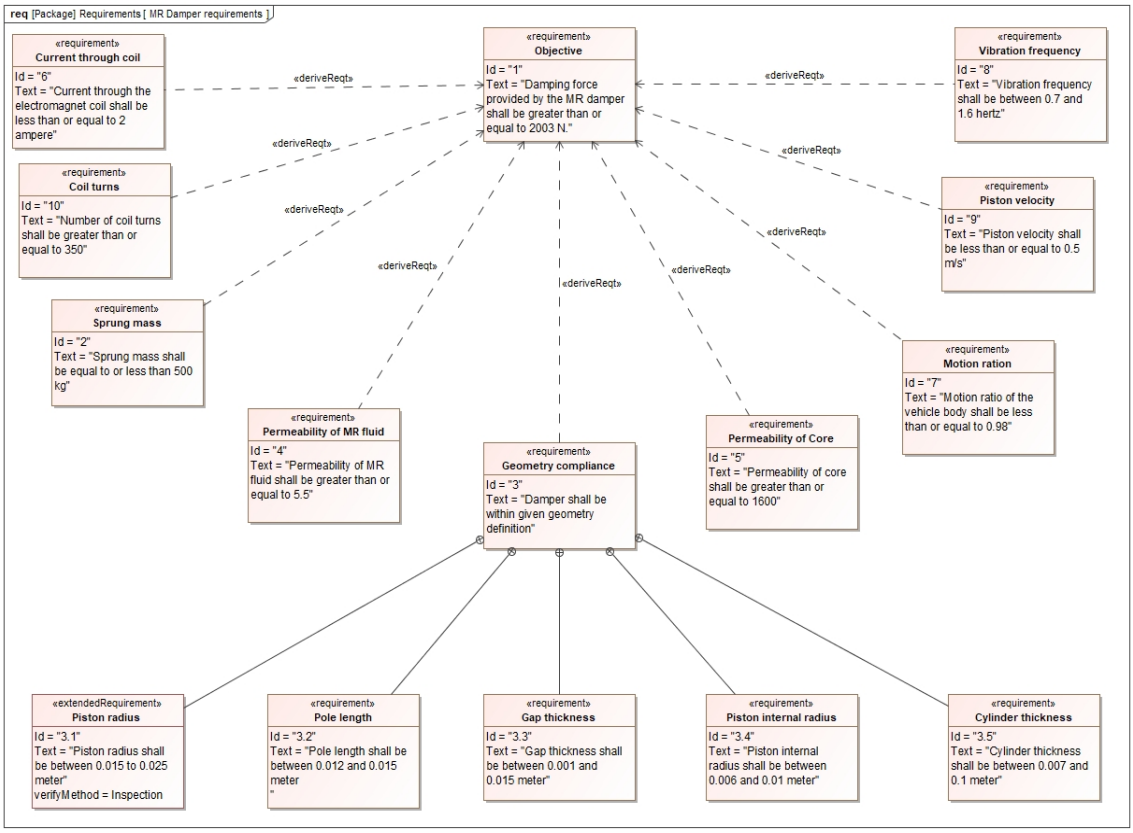

Fig. 7.8. Requirements diagram for MR damper design using MagicDraw system modeler

7.3.2 Block Definition Diagram (BDD)

The block definition diagram for the Magneto-rheological damper- damping force determination is shown in Figure 7.9. The diagram represents all the subsystems, which are related to the MR damper. The subsystem considered in the MBSE block definition diagram are derived from FAST and boundary diagram.

Fig. 7.9. Block definition diagram for MR damper design using MagicDraw system modeler

7.3.3 Internal Block Diagram

The internal definition diagram for the Magneto-rheological damper- damping force determination is shown in Figure 7.10. The diagram represents all the subsystems and interactions of MR damper. The subsystem and interactions considered in the MBSE internal diagram are derived from boundary diagram.

7.3.4 Parametric Diagram with MATLAB Integration

Parametric diagram is developed for the parametric determination of the following parameters of MR:

- Length of the electromagnet links
- Area of the electromagnetic links
- Magnetic flux through each link
- Total magnetic flux
- Flux density
- Permeability of the MR fluid and electromagnet

Parametric diagram of MR damper is shown in the Figure 7.11. Also, the simulation of the developed model is carried out using the MATLAB and the requirement traceability is performed. The green highlight on the interaction line shows that all MR damper design requirements are satisfied. Figure 7.12 shows the requirement traceability of MR damper. The designed and optimized MR damper is successfully designed using the system engineering techniques and validation is done using the parametric calculations through MATLAB algorithm integration.

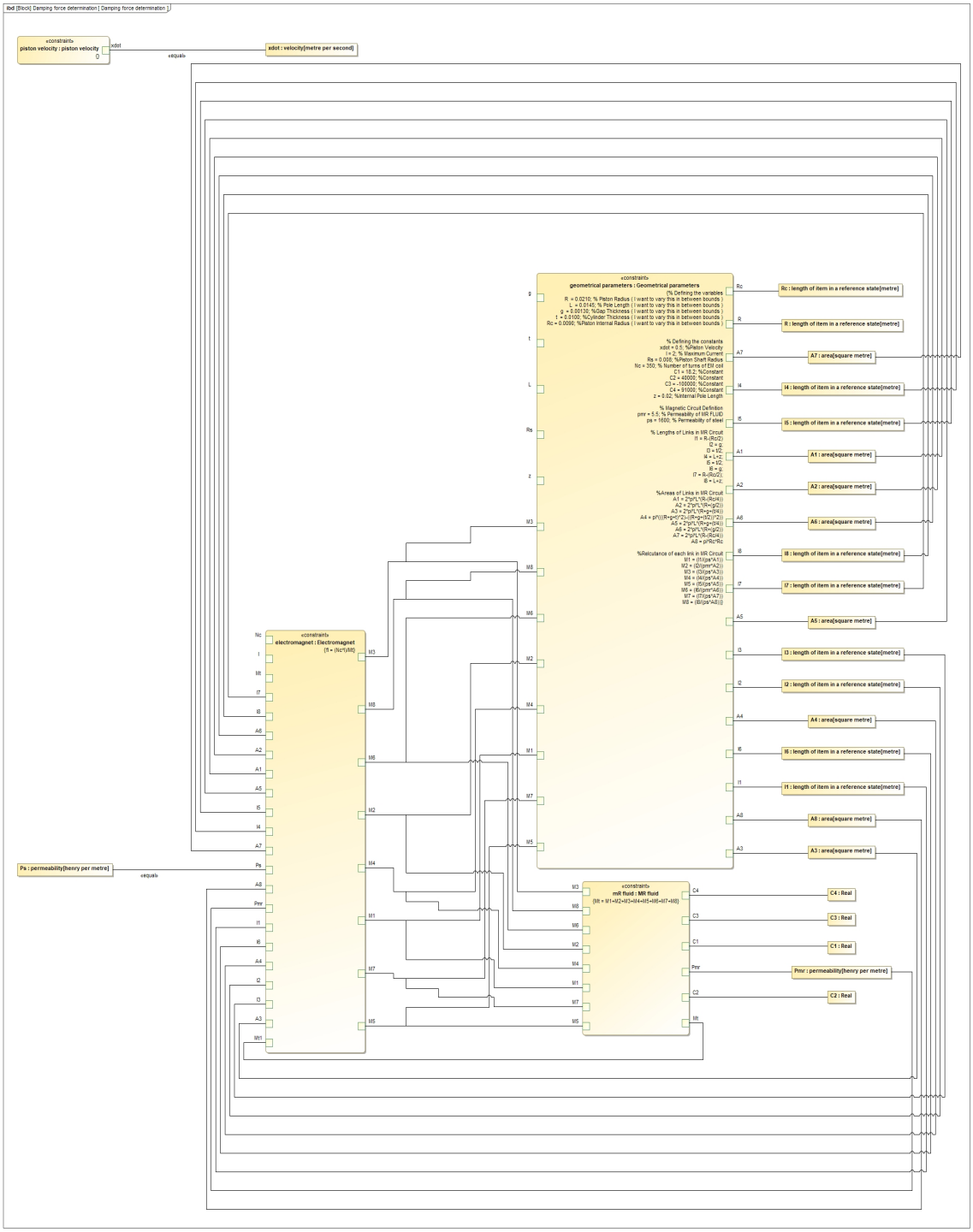

Fig. 7.10. Internal block diagram for MR damper design using MagicDraw system modeler

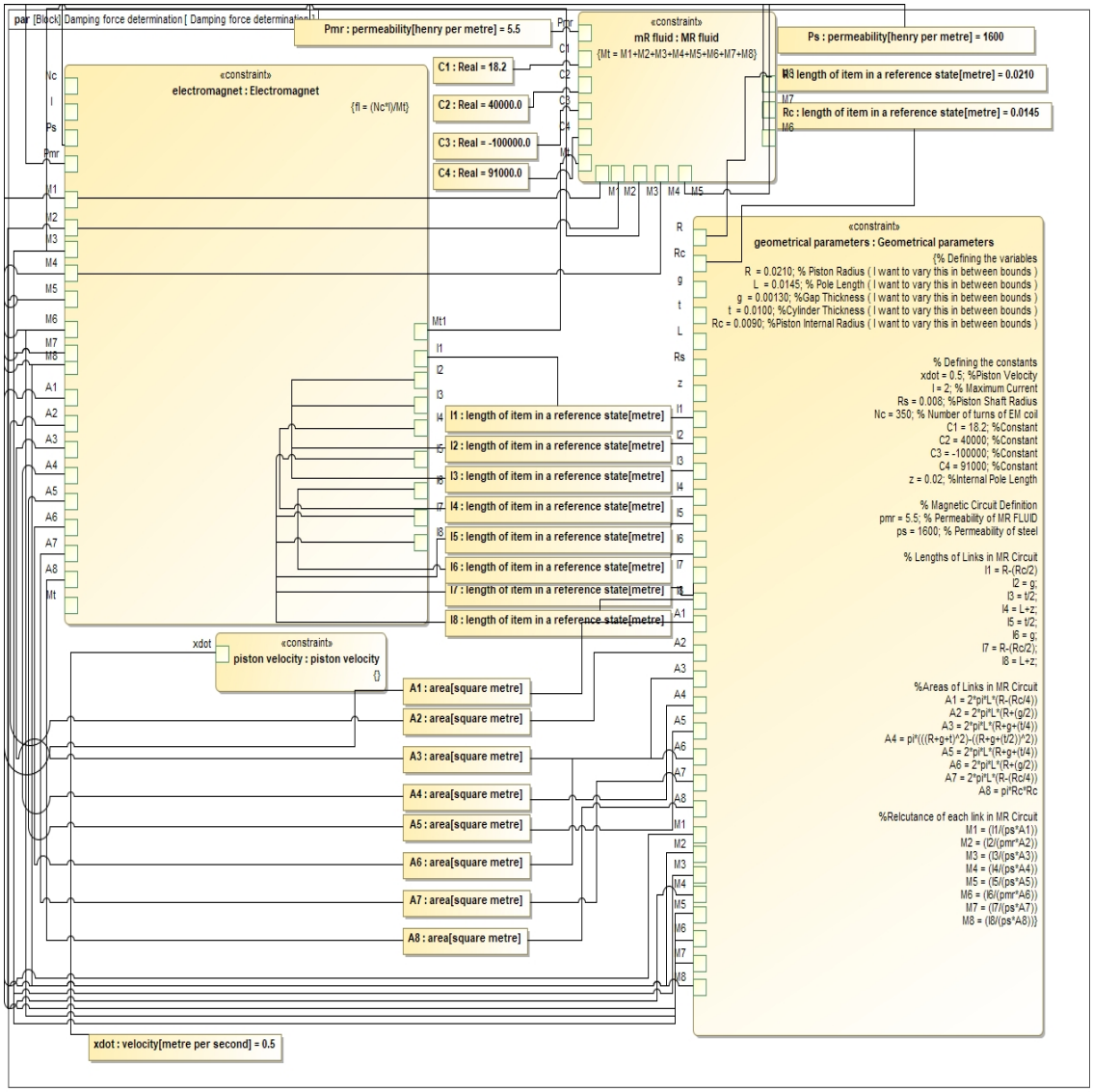

Fig. 7.11. Parametric diagram for MR damper design using MagicDraw system modeler

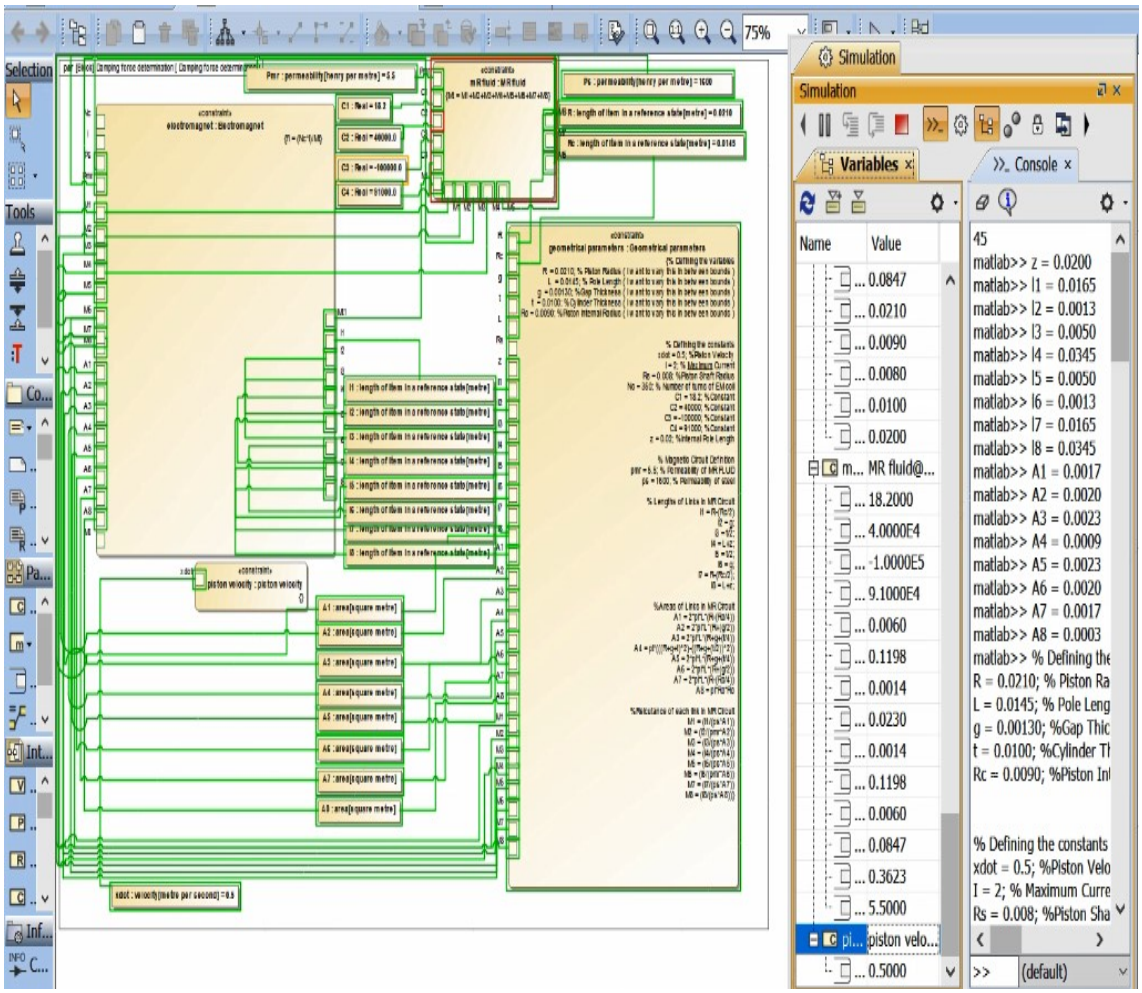

Fig. 7.12. Parametric diagram with requirement traceability for MR damper design using MagicDraw system modeler

7.4 Closure on the Chapter

Chapter 7 summarizes the systems engineering approach taken towards the MR damper design. FAST diagram is successfully used to determine the system level, subsystem level, and component level requirements. Multi layered FAST approach is used for the high level system requirement decomposition into component level requirements. Requirements determination is followed by the subsystem and interface determination using the boundary diagram. Flow streaming map is used to identify the data flow between different subsystems of system, and components of each subsystem. MBSE model for MR damper is modeled using requirements diagram, block definition diagram, internal block diagram, and parametric diagram. Further, system parameters generated by parametric diagram simulation is verified against the system requirement. The requirement traceability shows the viability and feasibility of the designed MR damper system for active suspension considering the Bouc-Wen hysteresis. Results obtained through parametric diagram simulation exactly matches the MATLAB algorithm results. Chapter 8 dicusses the open loop simulation, closed loop simulation with PID controller, and MBSE results in more detailed manner.

8. SUMMARY AND CONCLUSION

8.1 Results and Discussion

Present research successfully compares the analytical design of the passive suspension and active suspension using the Bingham hysteresis, Dahl hysteresis, and the Bouc-Wen hysteresis models using the MATLAB/Simulink package. The models are analyzed using six different road profiles to determine the most efficient and accurate model with minimum overshoot, least settling time, and maximum damping factor for the quarter car active suspension design. Tables 8.1 and 8.2 show the comparison of all the models with passive suspension. The statistics shows that the Bouc-Wen models is the superior model compared to all other models, considering sprung mass acceleration, overshoot, settling time, logarithmic decrement of spring mass vibration, and damping factor.

Table 8.1.
Sprung mass acceleration, overshoot, and settling time comparison of other models with respect to the passive suspension performance

Model	**Sprung mass acceleration comparison with respect to Passive suspension**	**Settling time comparison with respect to Passive suspension**	**Overshoot comparison with respect to Passive suspension**
Bingham	1.84%	36.15%	2.48%
Dahl	1.84%	56.07%	3.18%
Bouc-Wen	8.22%	88.31%	26.16%
Superiority	Bouc-Wen	Bouc-Wen	Bouc-Wen

Table 8.2.
Logarithmic Decrement and damping factor comparison of other models with respect to the passive suspension performance

Model	**Logarithmic Decrement comparison with respect to Passive suspension**	**Damping Factor comparison with respect to Passive suspension**
Bingham	67.58%	67.94%
Dahl	97.70%	98.35%
Bouc-Wen	390.11%	401.68%
Superiority	Bouc-Wen	Bouc-Wen

Table 8.3.
Damping force requirement through analytical calculation and MATLAB simulation

	Analytical calculation	**MATLAB simulation**
Damping force requirement (N)	1955.52	2003

The results show that the Bouc-Wen model is most efficient and the apt model for the design of the active suspension system. Further analysis is performed to determine the required maximum damping force under the utmost road disturbance to wheel. The MR damper is successfully designed and analytical results are then verified with the MATLAB simulation results, which shows 97.63 percent agreement between two. Table 8.3 shows the analytically determined value and MATLAB simulation for the damping force.

The geometric parameters of the damper are then optimized to develop the maximum required damping force and multi-objective optimization is successfully done with the pattern search approach. Sensitivity analysis is performed to determine

the sensitivity of all the five critical parameters, and vindicated with the simulation results that gap thickness is the most sensitive parameter for the damper design considering the maximum damping force requirement. Further, PID controller is implemented to reduce the sprung mass acceleration overshoot and more stability of vehicle is achieved. The overshoot improvement due to the PID controller implementation is summarized in Table 8.4 for the considered road profiles. The overshoot improvement observed for the different road profiles is in the range of 19.89 percent-81.96 percent for the constant settling time of 5 seconds. Logarithmic decrement and damping factor determines the disturbance experience by the vehicle sprung mass and the duration to diminish the disturbances. Bouc-Wen model is further analyzed for the logarithmic decrement and damping factor calculation. The model is analyzed for the two road profiles, which exhibit the property of logarithmic decrement. The logarithmic decrement and damping factor of Bouc-Wen for the step and sine road input is shown in the Table 8.5.

Table 8.4.
Percentage overshoot improvement of controlled response over uncontrolled response for all considered road profiles

Road input	**Uncontrolled response overshoot**	**Controlled response overshoot**	**Percentage improvement in overshoot**
Step	68.97	30.85	55.27
Sine	22.39	4.039	81.96
White noise	3.271	1.424	56.47
Uniform random number	113.4	43.55	61.60
Mixed road input	112.6	43.34	61.50
Road type C	5.019	4.121	17.89

The suitability of Bouc-Wen model is observed through uncontrolled as well as controlled responses. Active MR suspension with Bouc-Wen hysteresis theory is then

Table 8.5.
Bouc-Wen model logarithmic decrement and damping factor for step and sine wave input

Road input	**Logarithmic decrement**	**Damping factor**
Step	0.1988	1.2743
Sine	0.1429	0.9069

modeled using the systems engineering techniques explained in section 7.2. Section 7.3 documents the successful MBSE model development for MR damper optimized in secion 4.4. The unique multidisciplinary integrated approach of systems engineering and control system engineering is applied towards this research. Results discussed above vindicates the successful design, Modeling, and simulation of active suspension MR damper.

8.2 Future Scope

The present work shows the non-linear modeling of active suspension with MR damper considering Bingham, Dahl, and Bouc-wen model. The multi objective design optimization of MR damper has done with pattern search approach. The controlled response obtained with PID implementation for designed system shows improved results over other considered system. MBSE model is developed for the designed system considering systems engineering tool. The results can be further enhanced with the following approaches:

- The active suspension model developed in this research is compatible for real time target deployment. Code generation is achieved with the developed model. The physical testing setup for the designed MR damper and active suspension control logic validation can compensate for the assumption made during model based simulation.

- An optimal control algorithm for designed non-linear suspension system can give more robust and accurate behavior. Optimal control theories such LQG-LQR, Model predictive control (MPC) will result into better dynamic control for sprung mass displacement minimization against the road surface disturbance.

- MBSE model developed in the research can be further integrated with product lifecycle management tools such as Siemens PLM. The integration will prove into the better project management for the product under consideration. Also, integration will result into application system engineering management principle and can give thorough system engineering approach.

8.3 Closure on the Chapter

Chapter 8 documents the uncontrolled response comparison for determination of desired active MR suspension hysteresis model. The statistical data for overshoot, settling time, sprung mass acceleration, logarithmic decrement, and damping factor shows the comparison of each considered hysteresis model with passive suspension as base model. Also, section 8.1 documents the statistical data for response improvement due to PID controller implementation through uncontrolled and controlled response comparison for Bouc-Wen model. Systems engineering approach has been implemented for the active suspension damper design and requirement traceability.

REFERENCES

REFERENCES

[1] Q. Nguyen, S. Choi, Y. Lee, and M. Han, "An analytical method for optimal design of mr valve structures," *Smart Materials and Structures*, vol. 18, no. 9, p. 095032, 2009.

[2] B. Sapiński and J. Filuś, "Analysis of parametric models of mr linear damper," *Journal of Theoretical and Applied Mechanics*, vol. 41, no. 2, pp. 215–240, 2003.

[3] G. Hu, F. Liu, Z. Xie, and M. Xu, "Design, analysis, and experimental evaluation of a double coil magnetorheological fluid damper," *Shock and Vibration*, vol. 2016, 2016.

[4] M. Lita, N. C. Popa, C. Velescu, and L. N. Vekas, "Investigations of a magnetorheological fluid damper," *IEEE Transactions on Magnetics*, vol. 40, no. 2, pp. 469–472, 2004.

[5] U. Dogruer, F. Gordaninejad, and C. A. Evrensel, "A new magneto-rheological fluid damper for high-mobility multi-purpose wheeled vehicle (hmmwv)," *Journal of Intelligent Material Systems and Structures*, vol. 19, no. 6, pp. 641–650, 2008.

[6] W. H. El-Aouar, "Finite element analysis based modeling of magneto rheological dampers," pp. 1–119, 2002.

[7] E. Rubel, K.-H. Haegele, M. Panther, and K. Gatter, "Semi-active suspension control," Feb. 23 1993, uS Patent 5,189,615.

[8] V. Lampaert, F. Al-Bender, and J. Swevers, "A generalized maxwell-slip friction model appropriate for control purposes," in *Physics and Control, 2003. Proceedings. 2003 International Conference*, vol. 4. IEEE, 2003, pp. 1170–1177.

[9] H.-g. Li and G. Meng, "Nonlinear dynamics of a sdof oscillator with bouc–wen hysteresis," *Chaos, Solitons & Fractals*, vol. 34, no. 2, pp. 337–343, 2007.

[10] S. S. Rao and F. F. Yap, *Mechanical vibrations*. Prentice Hall Upper Saddle River, 2011, vol. 4.

[11] Q. Zhou, "Research and simulation on new active suspension control system," Ph.D. dissertation, Lehigh University, 2013.

[12] A. Tandel, A. Deshpande, S. Deshmukh, and K. Jagtap, "Modeling, analysis and pid controller implementation on double wishbone suspension using simmechanics and simulink," *Procedia Engineering*, vol. 97, pp. 1274–1281, 2014.

[13] A. E.-N. S. Ahmed, A. S. Ali, N. M. Ghazaly, and G. A. El-Jaber, "Pid controller of active suspension system for a quarter car model," *International Journal of Advances in Engineering & Technology*, vol. 8, no. 6, p. 899, 2015.

[14] H. Wissam and Y. Turki, "Quarter car active suspension system control using fuzzy controller tuned by pso," *International Journal of Computer Applications*, vol. 127, no. 2, pp. 38–43, 2015.

[15] D. Hanafi, "The quarter car fuzzy controller design based on model from intelligent system identification," in *Industrial Electronics & Applications, 2009. ISIEA 2009. IEEE Symposium on*, vol. 2. IEEE, 2009, pp. 930–933.

[16] A. Çakan, F. M. Botsalı, and M. Tinkir, "Modeling and controller comparison for quarter car suspension system by using pid and type-1 fuzzy logic," in *Applied Mechanics and Materials*, vol. 598. Trans Tech Publ, 2014, pp. 524–528.

[17] M. Heidari and H. Homaei, "Design a pid controller for suspension system by back propagation neural network," *Journal of Engineering*, vol. 2013, 2013.

[18] M. Zeinali, S. A. Mazlan, A. Y. A. Fatah, and H. Zamzuri, "A phenomenological dynamic model of a magnetorheological damper using a neuro-fuzzy system," *Smart Materials and Structures*, vol. 22, no. 12, p. 125013, 2013.

[19] R. S. Peak, R. M. Burkhart, S. A. Friedenthal, M. W. Wilson, M. Bajaj, and I. Kim, "9.3. 3 simulation-based design using sysml part 2: Celebrating diversity by example," in *INCOSE International Symposium*, vol. 17, no. 1. Wiley Online Library, 2007, pp. 1536–1557.

[20] T. Johnson, A. Kerzhner, C. J. Paredis, and R. Burkhart, "Integrating models and simulations of continuous dynamics into sysml," *Journal of Computing and Information Science in Engineering*, vol. 12, no. 1, p. 011002, 2012.

[21] J. W. Gravatt, "Magneto-rheological dampers for super-sport motorcycle applications," pp. 1–90, 2003.

[22] W. Dave, "The other active suspension cars - leyton house," pp. 1–6, June 2015. [Online]. Available: https://www.f1technical.net/forum/viewtopic.php?t=21478start=45

[23] J.-H. Koo, F. D. Goncalves, and M. Ahmadian, "A comprehensive analysis of the response time of mr dampers," *Smart materials and structures*, vol. 15, no. 2, p. 351, 2006.

[24] V. Rouillard and M. A. Sek, "Synthesizing nonstationary, non-gaussian random vibrations," *Packaging Technology and Science*, vol. 23, no. 8, pp. 423–439, 2010.

[25] N. Kwok, Q. Ha, M. Nguyen, J. Li, and B. Samali, "Bouc–wen model parameter identification for a mr fluid damper using computationally efficient ga," *ISA transactions*, vol. 46, no. 2, pp. 167–179, 2007.

[26] J. Sun and Y. Sun, "Comparative study on control strategy of active suspension system," in *Measuring Technology and Mechatronics Automation (ICMTMA), 2011 Third International Conference on*, vol. 1. IEEE, 2011, pp. 729–732.

[27] A. Aldair and W. Wang, "Design an intelligent controller for full vehicle nonlinear active suspension systems," *International journal on smart sensing and intelligent systems*, vol. 4, no. 2, pp. 224–243, 2011.

[28] M. Giaraffa, "Tech tip: Springs & dampers, part one," *Optimum G technical papers*, pp. 1–4, 2012.

[29] S. P. Deshmukh, H. Zambare, K. Mate, M. S. Shewale, and Z. Khan, "System identification and pid implementation on double flexural manipulator," in *Nascent Technologies in the Engineering Field (ICNTE), 2015 International Conference on*. IEEE, 2015, pp. 1–5.

[30] L. Fu and P. Li, "The research survey of system identification method," in *Intelligent Human-Machine Systems and Cybernetics (IHMSC), 2013 5th International Conference on*, vol. 2. IEEE, 2013, pp. 397–401.

[31] J. Nováková, "Dynamic system identification methods for fmri data processing," Ph.D. dissertation, Czech Technical University in Prague, 2013.

[32] P. Liu, E. N. Pistikopoulos, and Z. Li, "An energy systems engineering approach to the optimal design of energy systems in commercial buildings," *Energy Policy*, vol. 38, no. 8, pp. 4224–4231, 2010.

[33] Z. Zhou, P. Liu, Z. Li, and W. Ni, "An engineering approach to the optimal design of distributed energy systems in china," *Applied Thermal Engineering*, vol. 53, no. 2, pp. 387–396, 2013.

[34] P. Liu, M. C. Georgiadis, and E. N. Pistikopoulos, "An energy systems engineering approach for the design and operation of microgrids in residential applications," *Chemical Engineering Research and Design*, vol. 91, no. 10, pp. 2054–2069, 2013.

[35] F. Milella, "Problem-solving by immersive virtual reality: Towards a more efficient product emergence process in automotive," *Journal of Multidisciplinary Engineering Science and Technology*, vol. 2, no. 4, pp. 860–867, 2015.

[36] S. Friedenthal, A. Moore, and R. Steiner, *A practical guide to SysML: the systems modeling language*. Morgan Kaufmann, 2014.

[37] H. Kim, D. Fried, P. Menegay, G. Soremekun, and C. Oster, "Application of integrated modeling and analysis to development of complex systems," *Procedia Computer Science*, vol. 16, pp. 98–107, 2013.

[38] H. Kim, D. Fried, P. Menegay, and G. Soremekun, "Integrated modeling and analysis to support model-based systems engineering," in *Proceedings of the ASME 2012 11th Biennial Conference on Engineering Systems Design and Analysis, ESDA*, vol. 83017, 2012, pp. 2–4.

[39] G. Bleakley, A. Lapping, and A. Whitfield, "6.6. 2 determining the right solution using sysml and model based systems engineering (mbse) for trade studies," in *INCOSE International Symposium*, vol. 21, no. 1. Wiley Online Library, 2011, pp. 783–795.

[40] F. Mhenni, J.-Y. Choley, O. Penas, R. Plateaux, and M. Hammadi, "A sysml-based methodology for mechatronic systems architectural design," *Advanced Engineering Informatics*, vol. 28, no. 3, pp. 218–231, 2014.

[41] C.-J. Sjöstedt, "Modeling and simulation of physical systems in a mechatronic context," Ph.D. dissertation, KTH, 2009.

[42] M. Bendaoud, C. Lecomte, and B. Yannou, "A methodological framework to design and assess food traceability systems," *International Food and Agribusiness Management Review*, vol. 15, no. 1, pp. 103–125, 2012.

[43] U. Yildirim and F. Campean, "An enhanced interface analysis method for engineering change management," in *Smart Product Engineering*. Springer, 2013, pp. 191–200.

[44] T. R. Browning, "Applying the design structure matrix to system decomposition and integration problems: a review and new directions," *IEEE Transactions on Engineering management*, vol. 48, no. 3, pp. 292–306, 2001.

[45] C.-O. Wene, "Energy-economy analysis: linking the macroeconomic and systems engineering approaches," *Energy*, vol. 21, no. 9, pp. 809–824, 1996.

[46] S. Nag, "Satellite constellation mission design using model-based systems engineering and observing system simulation experiments," pp. 1–12, 2014.

[47] N. Snyder and M. Antkowiak, "Applying systems engineering in a renewable energy research & development environment," in *INCOSE International Symposium*, vol. 20, no. 1. Wiley Online Library, 2010, pp. 2422–2429.

[48] D. Goubet, J. Fauroux, and G. Gogu, "Gripping mechanisms in current wood harvesting machines," *Frontiers of Mechanical Engineering*, vol. 8, no. 1, pp. 42–61, 2013.

[49] Q. Shen, J. K. Chung, H. Li, and L. Shen, "A group support system for improving value management studies in construction," *Automation in Construction*, vol. 13, no. 2, pp. 209–224, 2004.

[50] R. Cressent, V. Idasiak, and F. Kratz, "Model-based systems engineering with sysml for reliable systems design," *INSIGHT*, vol. 14, no. 4, pp. 18–20, 2011.

[51] M. dos Santos Soares and J. L. Vrancken, "Model-driven user requirements specification using sysml." *JSW*, vol. 3, no. 6, pp. 57–68, 2008.